The Journal of Chemical Physics

RESEARCH ARTICLE | SEPTEMBER 19 2023

Neutral gas pressure dependence of ion–ion mutual neutralization rate constants using Landau–Zener theory coupled with trajectory simulations

Zhibo Liu; Mrittika Roy ; Nathan J. DeYonker ; Ranganathan Gopalakrishnan

J. Chem. Phys. 159, 114111 (2023)
https://doi.org/10.1063/5.0168609

The Journal of Chemical Physics ARTICLE pubs.aip.org/aip/jcp

Neutral gas pressure dependence of ion–ion mutual neutralization rate constants using Landau–Zener theory coupled with trajectory simulations

Cite as: J. Chem. Phys. 159, 114111 (2023); doi: 10.1063/5.0168609
Submitted: 19 July 2023 • Accepted: 28 August 2023 •
Published Online: 19 September 2023

Zhibo Liu,[1] Mrittika Roy,[1] Nathan J. DeYonker,[2] and Ranganathan Gopalakrishnan[1,a)]

AFFILIATIONS

[1] Department of Mechanical Engineering, The University of Memphis, Memphis, Tennessee 38152, USA
[2] Department of Chemistry, The University of Memphis, Memphis, Tennessee 38152, USA

[a)] **Author to whom correspondence should be addressed:** rgplkrsh@memphis.edu

ABSTRACT

In this computational study, we describe a self-consistent trajectory simulation approach to capture the effect of neutral gas pressure on ion–ion mutual neutralization (MN) reactions. The electron transfer probability estimated using Landau–Zener (LZ) transition state theory is incorporated into classical trajectory simulations to elicit predictions of MN cross sections in vacuum and rate constants at finite neutral gas pressures. Electronic structure calculations with multireference configuration interaction and large correlation consistent basis sets are used to derive inputs to the LZ theory. The key advance of our trajectory simulation approach is the inclusion of the effect of ion-neutral interactions on MN using a Langevin representation of the effect of background gas on ion transport. For $H^+ - H^-$ and $Li^+ - H(D)^-$, our approach quantitatively agrees with measured speed-dependent cross sections for up to ~10^5 m/s. For the ion pair $Ne^+ - Cl^-$, our predictions of the MN rate constant at ~1 Torr are a factor of ~2 to 3 higher than the experimentally measured value. Similarly, for $Xe^+ - F^-$ in the pressure range of ~20 000–80 000 Pa, our predictions of the MN rate constant are ~20% lower but are in excellent qualitative agreement with experimental data. The paradigm of using trajectory simulations to self-consistently capture the effect of gas pressure on MN reactions advanced here provides avenues for the inclusion of additional nonclassical effects in future work.

I. INTRODUCTION

The *elementary* recombination of a positive ion $\boldsymbol{A}^+$ and a negative ion $\boldsymbol{B}^-$ in the presence of neutral background gas molecules $\boldsymbol{M}$ leads to a ternary interaction of the form

$\boldsymbol{A}^+ + \boldsymbol{B}^- + \boldsymbol{M} \rightarrow \boldsymbol{AB} + \boldsymbol{M}$, termed ion–ion recombination (IIR) and $\boldsymbol{A}^+ + \boldsymbol{B}^- + \boldsymbol{M} \rightarrow \boldsymbol{A} + \boldsymbol{B} + \boldsymbol{M}$, termed ion mutual neutralization (MN).

An electron transfer from $\boldsymbol{B}^-$ to $\boldsymbol{A}^+$ replaces the ionic reactants $\boldsymbol{A}^+, \boldsymbol{B}^-$ with neutral products $\boldsymbol{AB}$ or $\boldsymbol{A}, \boldsymbol{B}$. IIR or MN reactions (collectively denoted as MN reactions in this article) are a key step in the chemical dynamics of ionized gas environments,[1–6] such as flames, plasmas, detonations, as well as in cosmic gas clouds. For instance, (1) ionization of neutrals by solar and cosmic radiation and their subsequent recombination are one of the sources of new aerosol particles that act as cloud condensation nuclei in the atmosphere,[7–11] (2) in combustion environments, recombination reactions generate energetic photons and hot neutrals that provide the pathway for energy transfer out of the reaction volume, (3) ion–ion recombination that is responsible for removing ion pairs, along with other ionic processes, determines the energy balance, chemical composition, and stability of plasmas construed as ionized gas-phase systems, such as flames,[12] discharges,[11] atmosphere,[13,14] rare gas-halide lasers,[15] dielectric insulating gases,[16] and dusty plasmas.[17]

In the last few decades, experiments and modeling investigations have been conducted in the free-molecular or vacuum limit and the MN process is less extensively studied at near or beyond

atmospheric pressure even though the measured rate constants show a clear pressure dependency.[18] For reactions relevant for energy systems such as flames, plasmas, and detonations that operate at atmospheric pressures or beyond, experiments involving polyatomic species with a plasma afterglow chamber setup are typically utilized for plasma generation or ionization followed by a series of time lapse measurement of number density profile that can be later used for constructing the MN rate constant.[19] On the other hand, several experiments have been conducted to measure the MN cross section in the free-molecular limit for a range of ion relative velocities using merged-beam-type experimental apparatus.[20–27] MN reactions between rare gas cations ($He^+, Ne^+, Ar^+, Kr^+, Xe^+$) and halide anions ($Cl^-, Br^-, I^-$) have been systematically studied in the pressure range of ~0.5–2 Torr in the work of Viggiano *et al.*[15,28] using a Flowing Afterglow-Langmuir Probe (FALP) coupled to Variable Electron and Neutral Density Attachment Mass Spectrometry (VENDAMS) apparatus.[29–32] The Viggiano group has also reported the MN rate involving halide anions and polyatomic cations,[33,34] halide ions and hydrogen cations,[35] and rare gas cations and polyatomic anions.[29,36–38] In an earlier era, Smith's group studied many pairs of polyatomic ions using similar experimental techniques in the ~1 Torr pressure range.[39–43]

Olson[44] proposed an absorbing sphere model (ASM) that calculates the velocity-dependent recombination cross section for ion pairs by considering Coulombic and dipole–dipole interactions and the electron transfer probability as a function of radial separation between the anion and cation. The highlight of this model is the calculation of electron transfer probability self-consistently using the semiclassical Landau–Zener (LZ) two-state transition theory[45–47] that describes nonadiabatic transitions between quantum states based on the crossover of the potential energy curves (PECs) or surfaces of products and reactants. The recombination cross section is calculated as a function of the ion relative velocity by integrating the electron transfer probability over the distribution of ion impact parameters. ASM provided satisfactory agreement with experiments in vacuum for a wide range of nonrelativistic ion relative velocities.[23,27] This low-pressure limit is especially appealing to an application of LZ theory for two monoatomic species since the potential energy surface (PES) in such cases is reduced to a well-defined 1D potential energy curve (PEC) and there are only a handful of states interacting with deterministic nuclear motion at nonrelativistic speeds. The LZ theory employs three parameters (described in Sec. II later) calculated from the PEC or PES of an MN reaction and the relative speed of the species varied as a parameter in reaction cross section integrals or equivalently, obtained from classical trajectories simulations. The success and simplicity of ASM resulted in the calculation of inputs to the LZ theory for several IIR or MN reactions as well as charge transfer reactions between a monoatomic cation and an atom[48–50] involving the transfer of exactly one electron. In the limit of a large number of product states, Hickman[51] generalized the ASM to approximately explain the recombination rates of polyatomic ion pairs as well. More recently, Bopp, Miller, Viggiano, and Troe[52] used this approach to include the effects of rotation and vibration. Olson[53] succinctly summarizes ASM and applications to modeling of charge transfer reactions.

We draw inspiration from the classical approach to reaction rate constant or cross section modeling using the crossing of potential energy curves for elementary charge or excitation transfer.[54–58] ASM is an excellent starting point to self-consistently model IIR or MN reactions taking place at finite gas pressures if the effect of neutral collisions is included accurately. Due to the inherent difficulties in PES construction for polyatomic ion pairs, we defer their consideration to future investigations, and we focus on monoatomic ion pairs in this study and establish the methodology to capture the effect of pressure on their MN rate constant β. A trajectory simulations-based modeling approach suitable for low to atmospheric pressure and capturing the MN rate constant of monoatomic ions at moderate accuracy without losing the details of electron transfer is described herein. We use computational chemistry techniques for obtaining PECs that serve as input to the LZ theory and subsequently elicit predictions of the electron transfer probabilities incorporated into the ion trajectory simulations.

The principal methodology in the current study is based on the LZ theory that models the details of the transition between two quantum states. The advantage and simplicity of this method lies in the calculation of system-specific parameters that are related to electronic structure without ambiguities or free parameters. However, the disadvantage is that when system size (number of electrons) increases, for instance, a system of two polyatomic ions, the construction and computation of the PES are extremely computationally intensive and often impossible due to their multidimensional nature. Disregarding this principal difficulty, the LZ approach is still one of the most accessible semiclassical approaches for monoatomic species except for the systems where multiple states are interacting with each other.[45–47] For a finite pressure system, the effect of the neutral gas on ion trajectories is captured using a Langevin representation of the background gas molecules through the ion diffusion constant and ion friction factor.[59] The classical equations of motion to track the nuclei are integrated using a fourth-order Runge–Kutta method in the vacuum limit where the forces due to gas drag and thermal collisions vanish and a fourth-order Runge–Kutta method[60] for Langevin stochastic differential equations of motion[59] for cases where gas pressure is finite. Excellent agreement with Olson's theory is seen in the free-molecular regime for small monoatomic ion pairs such as $H^+ - H^-, He^+ - H^-, N^+ - O^-, O^+ - O^-, Li^+ - D^-$ and is applied to the low-pressure (~1 Torr) measurement of MN rate constant for $Ne^+ - Cl^-$. There is limited experimental data from afterglow experiments[18,61–63] in which rare gas cations recombined with halide ions and the $Xe^+ - F^-$ ion pair[61] is selected as a case study in our current study.

The rest of this article is organized as follows: We first describe the details of our calculation of MN probability using the Landau–Zener theory, followed by the steps of our Monte Carlo (MC) trajectory simulation in vacuum and Langevin Dynamics (LD) simulations at finite pressures. Subsequently, we present detailed electronic structure calculations for $H^+ - H^-$ ion pair and perform detailed benchmarking against prior electronic structure calculations and MN cross section data. Following that, we similarly present results for $Li^+ - H(D)^-$ pair and compare with the available fully quantum calculations and cross sections. Building complexity, we explore multi-electron systems such as $Ne^+ - Cl^-$ and then $Xe^+ - F^-$. For both these pairs, we calculate MN rate constants that are compared with experimental data. Finally, using published crossing distance and coupling constant data, we calculate cross sections for $He^+ - H^-, N^+ - O^-, O^+ - O^-$ to establish that our approach is tractable when accurate electronic structure calculations

are available. We conclude by reflecting on both the strengths and shortcomings of the current approach of incorporating nonclassical electron transfer probability into classical trajectory simulations as a modeling paradigm for describing the effect of gas pressure on MN.

II. METHODS

Ion–ion recombination can be broadly thought of as a two-step process as depicted in Fig. 1 that involves (1) Step 1—the transport of ions $\boldsymbol{A}^+$ and $\boldsymbol{B}^-$ toward each other driven by thermal energy ($\sim k_B T$) and potential interactions (Coulomb and van der Waals), and (2) Step 2—charge transfer between the two ions when they are sufficiently close leading to neutral product $\boldsymbol{AB}$ or mutual neutralization $\boldsymbol{A}, \boldsymbol{B}$ formation. The scope of this study is restricted to IIR or MN reactions that are transport-limited instantaneous electron transfer compared to the timescale of ion transport[64,65] and we do not consider slow charge (electron) transfer reactions. Ion transport is determined by the long-range attractive interaction (Coulombic $\sim r^{-1}$) between the oppositely charged ions, short-range attractive interaction (due to induced or permanent dipole-dipole $\sim r^{-4} - r^{-6}$), and very short-range repulsive interaction (due to electron degeneracy pressure $\sim r^{-12}$), where r is the separation between the ions. Ion–ion recombination in finite pressure systems is a ternary process wherein collisions with the neutral background gas molecules leads to loss of kinetic energy of the ions and facilitates the formation of a "bound ion pair." A bound ion pair is characterized by the relative kinetic energy being less than the attractive electrostatic potential energy (negative total energy) facilitating the close approach needed for charge transfer to take place and complete the recombination reaction.

A. Calculation of electron transfer probability p_{LZ}

Due to the quantum nature of electron transfer between two ions, a fixed physical boundary cannot be defined to characterize the velocity-dependent cross section $\sigma(v)$ for MN reactions (v is the ion relative speed) and the probability of MN reaction $P(b, v)$ needs to be integrated over the distribution of ion–ion collision impact parameter $b \in [0, \infty)$. Since each interaction between two ions involves at least one crossing when the ions approach each other and one when they are receding away, the adiabatic transition (electron transfer) probability $1 - p_{LZ}$ needs to be evaluated at each of the two crossing instances [Fig. 2(a)]. For a given b, v, the probability of MN $P(b, v) = 2p_{LZ}(1 - p_{LZ})$ for a single crossing system that includes an approach and a retreat leading to $P(b, v) \leq 0.5$. We invoke the LZ theory[45–47] to calculate p_{LZ} without resorting to computationally much more intensive *ab initio* solutions to Schrödinger's equation for the chemical systems considered in this study, namely monoatomic cation–anion pairs. LZ theory allows the calculation of the diabatic transition probability of a single passage p_{LZ} between two quantum states at the point of an avoided crossing[45–47] as depicted in Fig. 2(b) (note that adiabatic transition probability is $1 - p_{LZ}$),

$$p_{LZ} = \exp\left(\frac{-2\pi \mathrm{H}_{if}^2}{\hbar\left|\frac{\partial(E_2 - E_1)}{\partial t}\right|}\right), \tag{1}$$

where H_{if} is the electronic coupling between two states 1 and 2; E_1, E_2 are the energy of the two diabatic states at the crossing point. Following Olson, Peterson, and Moseley,[27] Eq. (1) is rewritten for an ion pair,

$$p_{LZ} = \exp\left(\frac{-2\pi \mathrm{H}_{if}^2}{\hbar\left|v_r(\vec{F}_2 - \vec{F}_1)\right|}\right), \tag{2}$$

where v_r is the radial component of the relative velocity $\vec{v}_2 - \vec{v}_1$ and $\vec{F}_2 - \vec{F}_1$ is the force difference at the crossing point. Equation (2) is strictly applicable for describing two state interactions/transitions

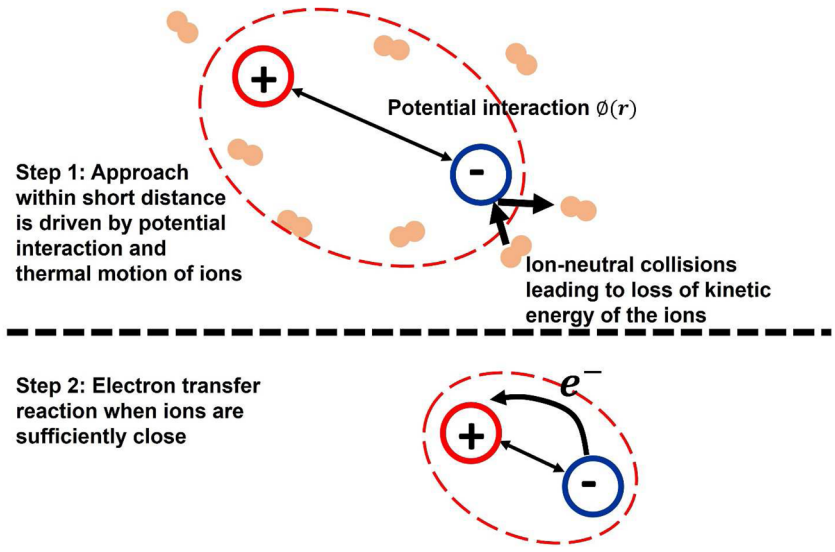

FIG. 1. Ion transport driven by potential interactions (Step 1) and fast electron transfer at close approach (Step 2).

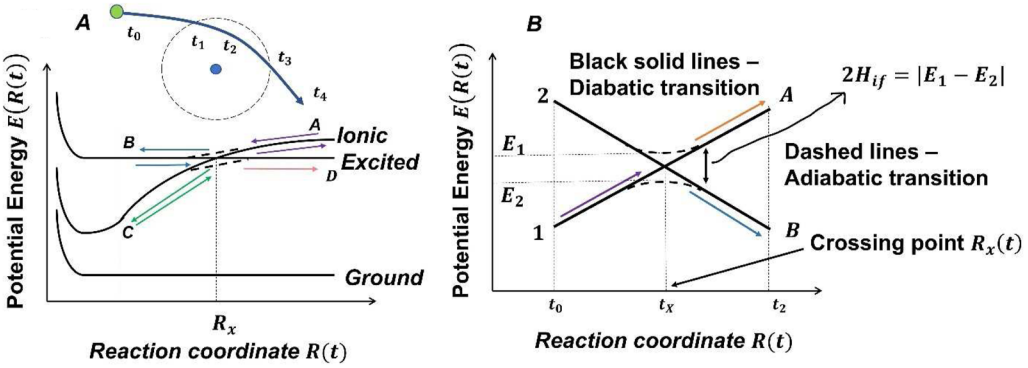

FIG. 2. (a) Schematic of an MN reaction in energy space for a single crossing system. Possible passages that lead to an MN reaction for ionic reactants starting from A and transition to state B (purple → blue → blue → pink) or diabatic transition to C and eventually to state D (purple → green → green → pink). The crossing point O is passed twice by the ions when approaching and receding away from each other. (b) Basic aspects of Landau–Zener (LZ) theory that describe the probability of transition between two quantum states of a chemical system.

only. If multiples states cross at the same point or if several two state crossings are closely spaced, the application of LZ theory becomes questionable. The applicability of the theory is best judged using the Nonadiabatic Coupling Matrix Element (NACME) calculations and the location of peak values of couplings. An ideal case is one in which the crossing points are free of multistate interactions and distinguishable from other two state couplings. This aspect will be discussed along with the PECs calculated for the ion pairs considered in this study.

B. MN cross section σ calculation in the free-molecular limit

In the free-molecular limit, the MN cross section can be calculated as

$$\sigma(v) = 2\pi \int_0^{b_c} bP(b,v)db, \tag{3}$$

where b_c is the critical impact parameter at which the outermost crossing point is still accessible. The complexity or the number of reaction paths increases rapidly as the number of crossings increase, and consequently, $P(b,v)$ is a nontrivial function and Eq. (3) needs to be evaluated numerically. This integral for a single crossing system can be evaluated analytically using tabulated H_{12} for various ion–ion and ion-neutral pairs.[27,48] As an alternative, the Monte Carlo trajectory simulation method is used here to evaluate $\sigma(v)$. By comparing with Olson's calculations, we show in this work that the Monte Carlo (MC) approach is equivalent to the analytical calculation for $\sigma(v)$ in the vacuum limit and is also amenable to the incorporation of additional physical effects that are analytically difficult to track, if not impossible.

The two-ion system is reduced to an equivalent reduced mass system where one of the ions is placed at the origin of a Cartesian coordinate system x,y,z and considered to be at rest. The relative trajectory of the other ion is simulated with a reduced mass $\mu = \frac{m_1 m_2}{m_1+m_2}$ as depicted in Fig. 3(a) (m_1, m_2 are ion masses),

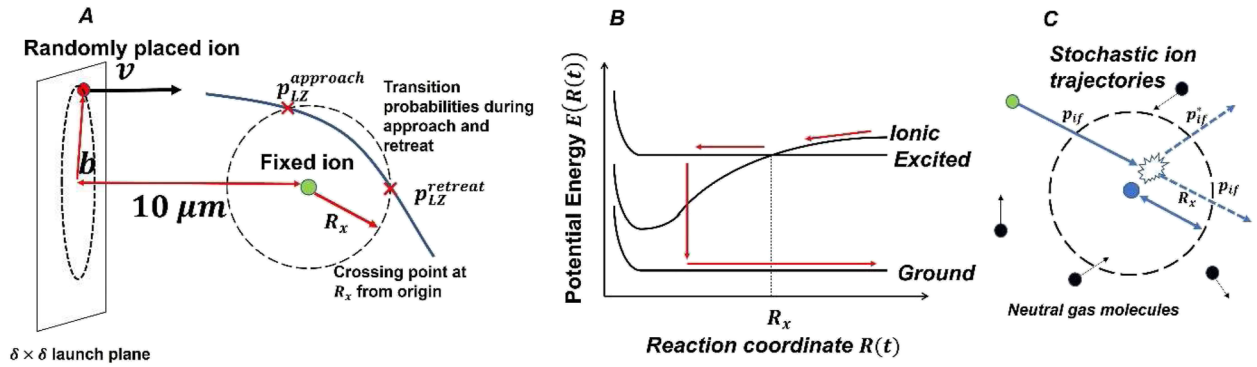

FIG. 3. (a) Schematic of the Monte Carlo (MC) trajectory simulation used for calculating the recombination cross section $\sigma(v)$ as a function of the ion relative speed v. (b) De-excitation of an excited species (formed from the MN of two ions) to ground state. (c) Collisions with neutral gas molecules scatter angular momentum and kinetic energy of the ions. The effect of gas molecules is implicitly represented using a Langevin model allowing the tracking of only the ions for MN modeling.

$$\mu \frac{d\vec{v}}{dt} = -\nabla \Phi, \tag{4a}$$

$$\Phi(\mathrm{r}) = -\frac{e^2}{4\pi\varepsilon_0 r} + 4\varepsilon_{12}\left[\left(\frac{\sigma_{12}}{r}\right)^{12} - \left(\frac{\sigma_{12}}{r}\right)^{6}\right], \tag{4b}$$

where $\Phi(r)$ is the ion–ion potential energy that comprises of Coulombic, van der Waals, and short-range repulsion terms; r is radial distance from the origin. The Lennard-Jones (LJ) parameters $\varepsilon_{12}, \sigma_{12}$ are calculated using the Lorentz–Berthelot rule as described in the supplementary material, Sec. S1-A. Equation (4) is integrated using the standard fourth-order Runge–Kutta method to track the ion position $\vec{r}(t)$ and velocity $\vec{v}(t)$. The Monte Carlo method calculates σ as a fraction of the area of a square from which the ion is launched toward the origin. The side of the square δ is set to $2b_c$ for a chosen v to ensure the accessibility of all LZ crossings. The plane is placed 10 μm from the origin to ensure that the ion starts without any significant force on it due to the other ion, and the ion is then launched from the starting plane with an initial velocity that is perpendicular to the plane and directed toward the origin. The starting point (x, y) is chosen randomly on the square and the impact parameter is then calculated as $b = \sqrt{x^2 + y^2}$. v is systematically varied over a desired range to calculate $\sigma(v)$ for comparison with available experimental data. A variable timestep $\Delta t = 0.0005 \times \min\left(\sqrt{\frac{r\mu}{F}}, \frac{r}{v}\right)$ is used, where F is the magnitude of the force and v is speed of the ion that is tracked using Eq. (4).

The overall or effective probability is decomposed into the probabilities of individual crossings for a given ion pair and a series of binary determinations are utilized for terminating a simulation trial, depicted in Fig. 2(a), when an adiabatic transition from ionic state to neutral state occurs with outgoing relative velocity (A → C → D) or the species are both in neutral states with their velocities receding from each other (A → B → D). The formed neutral states by the addition of an electron to the cation are almost never expected to be purely in the ground electronic state because those are much lower in energy compared to ionic states. The neutralization of the ions $\boldsymbol{A}^+, \boldsymbol{B}^-$ typically leads to the formation of an excited neutral $\boldsymbol{A}^*$ replacing the cation $\boldsymbol{A}^+$ and a ground state neutral $\boldsymbol{B}$ replacing the anion $\boldsymbol{B}^-$: $\boldsymbol{A}^+ + \boldsymbol{B}^- \rightarrow \boldsymbol{A}^* + \boldsymbol{B}$. De-excitation [Fig. 3(b)] by photon emission as well as through collisions with neutrals are possible, with the contribution of the latter increasing with gas pressure. Instead of a detailed discussion and incorporation of de-excitation physics, which is beyond the scope of the current study focused on modeling MN, we identify two limits of de-excitation:

(1) No de-excitation (de-excitation times are much longer than ion transport times): De-excitation has been neglected in the modeling of small monoatomic ions by Olson.[44] In this limit, we hypothesize that there exist pathways (transition probabilities) to access the same channel (crossing point) in the reverse or outgoing direction that led to their neutralization during approach. This leads to a finite probability for the system to re-ionize: $\boldsymbol{A}^* + \boldsymbol{B} \rightarrow \boldsymbol{A}^+ + \boldsymbol{B}^-$. The simulation runs until the formed neutral species A^*, B have velocities that are directed away and recede irreversibly from each other.

(2) Instantaneous de-excitation (de-excitation times are much shorter than ion transport times): The $\boldsymbol{A}^* \rightarrow \boldsymbol{A}$ transition takes place instantaneously and the simulation is terminated as soon as $\boldsymbol{A}^*$ is formed. The ground states $\boldsymbol{A}, \boldsymbol{B}$ do not typically have any energetic pathways to ionize again.

Kinetic studies on MN reactions typically measure the rate of disappearance of ions from an experimental volume. The reappearance of ions through the re-ionization of excited neutrals presents an additional nuance to the observed timeseries of ion concentrations from which rate constants are inferred. In the case of no de-excitation, the rate of depletion of ions is reduced compared to the case of instant de-excitation where excited neutrals have no pathway for forming ions again. The instantaneous de-excitation limit is likely to be unphysical in numerous circumstances and it only serves as an upper limit of the MN rate constant and should be used cautiously. We expect the no de-excitation limit to be a simple and closer representation of reality. Two sets of calculations for each of these limits are presented for the ion pairs considered. Future work is planned wherein unimolecular de-excitation kinetics via photoemission and ternary de-excitation through collisions with neutrals will be added to the simulation termination criteria.

At each crossing point, whether an electron is transferred in an ion → neutral or neutral → ion adiabatic transition is determined by comparing a uniformly distributed random number $\zeta \in (0, 1)$ with the transition probability $p_{LZ} : \zeta \geq p_{LZ}$.

N_{total} simulation runs are conducted until $N_{neu} = 8000$ trials of neutralization events are detected for numerical accuracy in the calculation of $\sigma(v)$ averaged over values of $b \in [0, \delta]$, equivalent to Eq. (3),

$$\sigma(v) = \delta^2 \frac{N_{neu}}{N_{total}}. \tag{5a}$$

Comparisons of $\sigma(v)$ through Eq. (5a) with pertinent experimental data are presented subsequently after describing the steps in determining the crossing point R_x and calculating the associated coupling parameter H_{if} for a given ion pair to be used in Eq. (2) for evaluating p_{LZ}. For a MN reaction that can proceed through M LZ channels or crossings, $N_{neu} = \sum_{i=1}^{M} N_i$. The fraction ζ_i of products formed through channel i can be obtained as $\zeta_i = \frac{N_i}{N_{neu}}$. The cross section σ_v averaged over the ion speed distribution may be computed repeating the above procedure for each v sampled from the Maxwell–Boltzmann speed distribution $\chi(v) = \sqrt{\frac{2}{\pi}}\left(\frac{\mu}{k_B T}\right)^{\frac{3}{2}} v^2 \exp\left(-\frac{\mu v^2}{2k_B T}\right)$ (k_B is the Boltzmann constant, and T is the temperature of the thermal bath),

$$\langle \sigma \rangle_v = \delta^2 \frac{\sum_{N_{neu}} v}{\sum_{N_{total}} v}, \tag{5b}$$

$\sum_{N_{neu}} v$ is the sum of the speeds that lead to an MN event and $\sum_{N_{total}} v$ is the sum of the speeds of all trials.

C. MN rate constant β calculation at finite gas pressures

The transition probability p_{LZ} is inherently stochastic due to the quantum nature of electron transfer that is captured using our MC implementation. At finite gas pressures, additional variability is introduced due to the thermal noise in ion position and velocity [Fig. 3(c)]. The time-resolved trajectory of the ions is coupled to the

electron transfer kinetics described by the semiclassical LZ theory by using the instantaneous ion (nuclear) position and velocity obtained from a purely classical trajectory simulation in the calculation of p_{LZ} using Eq. (2). Instead of σ, the MN rate constant β is calculated as a function of the gas pressure and temperature, in addition to ion composition. In the free-molecular limit, $\beta = \int_{v=0}^{v=\infty} \sigma(v) v \chi(v) dv$. In lieu of the MC method used in the vacuum limit, ion trajectories at finite gas pressures are simulated using the Langevin Dynamics (LD) method[59,66] to account for the effect of neutral gas on ion transport,

$$m\frac{d\vec{v}}{dt} = -f\vec{v} - \nabla\Phi + \vec{F}_B(t), \tag{6a}$$

$$\frac{d\vec{r}}{dt} = \vec{v}, \tag{6b}$$

where $\vec{r}$ is the ion position with respect to the origin of the cubical simulation domain of side L and $\vec{v}$ is the corresponding velocity measured with respect to an inertial frame of reference with origin at the center of the domain; f is the ion friction factor of ion; $\vec{F}_B$ is the stochastic force used to mimic the effect of thermal collisions between an ion and neutrals that is modeled as a Gaussian random vector with a time average of zero and autocorrelation given by

$$\int_0^{t_r} \vec{F}_B(t')dt' = 0, \tag{6c}$$

$$\int_0^{t_r} \vec{F}_B(t_r) \cdot \vec{F}_B(t' - t_r)dt' = 6fk_BT_g\delta(t_r), \tag{6d}$$

t_r is an arbitrary interval of time much longer than the ion momentum relaxation time $\sim \frac{m}{f}$ $\left(t_r \gg \frac{m}{f}\right)$; $-\nabla\Phi$ is the total electrostatic force on the ion; and Φ is the ion potential energy [Eq. (4b)] pairwise summed over all the other ions in the simulation. For systems at thermal equilibrium, the friction factor $f\left(\frac{kg}{s}\right)$, the ion (infinite-dilution) diffusion constant $D\left(\frac{m^2}{s}\right)$, and the ion low-field electrical mobility $\mu\left(\frac{m^2}{s \cdot V}\right)$ are related to each other through the fluctuation–dissipation theorem,[67]

$$D = \frac{\mu k_B T}{e} = \frac{k_B T}{f}, \tag{7}$$

where f for all the ions are calculated using the IMoS free-molecular ion mobility calculation package[68–70] that has been extensively validated against experimentally measured mobilities to a high degree of reliability[71,72] and are tabulated in Sec. S1-B. To simulate dilute ion concentrations, ions in the simulation are initialized sufficiently far away from each other so that their Coulombic potential energy $\frac{e^2}{4\pi\varepsilon_0 r_{MID}}$ is 100 times smaller than their nominal thermal energy $\frac{3}{2}k_BT$. The mean inter-ion spacing r_{MID} is selected as $r_{MID} = 100\frac{e^2}{4\pi\varepsilon_0}\frac{2}{3k_BT}$ by setting the simulation box size L and the number of ion pairs simulated $\frac{N}{2}$. $\frac{N}{2}$ is chosen as four ion pairs simulated in a run to observe neutralization events. L is computed as $L = 100N^{\frac{1}{3}}\frac{e^2}{4\pi\varepsilon_0}\frac{2}{3k_BT}$. The $\frac{N}{2}$ pairs of ions are initialized in the domain following a uniform distribution of positions and velocities sampled from the Maxwell–Boltzmann velocity distribution. Each of the N ions is tracked using Eq. (6) numerically integrated using a fourth-order Runge–Kutta method[60] for linear stochastic differential equations. Time step $\Delta t = 0.002 \times \min\left(\frac{r_{\min}}{v_{\max}}, \min\left(\sqrt{\frac{m_i r_{\min}}{F_{\max}}}\right), \left(\frac{m_i^2 r_{\min}^2}{f_i k_B T}\right)^{\frac{1}{3}}\right)$ is calculated using the minimum separation $r_{\min}$ among the $\frac{N(N-1)}{2}$ (monoatomic) ion pairs, maximum force $F_{\max}$, and speed $v_{\max}$ among N ions (m_i and f_i are the mass and friction factor of the ith ion, respectively). The dilute ion concentrations allow us to use the LZ crossing check in a pairwise fashion following the same logic used in the free-molecular limit while simulating one ion pair. Three- or higher-body collisions were extremely rare and were not included for analysis.

At finite pressures, especially near atmospheric pressure, due to significant damping of ion motion by the neutral gas, a pair of ions are likely to form a pseudo-stable orbit that eventually leads to a strong and unphysical bonding due to electrostatic attraction. Once a reasonably stable orbit is established, it is conceivable that eventually the ions will exchange an electron through close approach in pathways that are not amenable for description by the LZ theory. To account for such events, the simulation trial is terminated if the following condition is satisfied at a given radial separation between the ions r, v is the magnitude of their relative velocity, and μ is their reduced mass,

$$-\frac{e^2}{4\pi\varepsilon_0}\left(\frac{1}{R_{x,\min}} - \frac{1}{r}\right) + 4\varepsilon_{12}\left[\left(\frac{\sigma_{12}}{r}\right)^{12} - \left(\frac{\sigma_{12}}{r}\right)^{6}\right] - \frac{3}{2}k_BT \geq \frac{1}{2}\mu v^2, \tag{8}$$

$-\frac{e^2}{4\pi\varepsilon_0}\left(\frac{1}{R_{x,\min}} - \frac{1}{r}\right) + 4\varepsilon_{12}\left[\left(\frac{\sigma_{12}}{r}\right)^{12} - \left(\frac{\sigma_{12}}{r}\right)^{6}\right]$ is the energy necessary for accessing the closest LZ crossing distance $R_{x,\min}$, and $\frac{3}{2}k_BT$ is the ion thermal energy due to the Langevin thermostat in Eq. (5). The simulation runs until a total of 2000 terminations are detected due to ions either crossing LZ MN channels or forming bound orbits due to Coulombic attraction, which are eventually terminated using the criterion given by Eq. (8). An important feature of the LZ theory is that it is accurate to describe far-range electron transfers in Coulombic systems or crossings and does not describe short-range electron transfer in which the ions approach each other within the range of van der Waals attraction ($\sim r^{-6}$) and electron degeneracy repulsions ($\sim r^{-12}$) and/or if multiple crossings between different states are closely spaced in the PEC. We find that at vacuum or low pressures (~1 Torr), the neutralization terminations predominantly occur through one of the LZ crossings or paths for electron transfer. On the other hand, at high pressures (~1 atm), we find that the terminations are mostly through stable orbit formation and only a small fraction are through LZ crossings, see below. The MN rate constant $\beta\left(\frac{m^3}{s}\right)$ is calculated as

$$\beta = \frac{L^3}{\langle t \rangle}\left(\frac{N}{2}\right)^{-2}, \tag{9}$$

$\langle t \rangle$ is the mean neutralization time calculated as $\frac{\sum_i t_i}{M}$ where $\sum_i t_i$ is the sum of the neutralization times over $M = 2000$ trials. $\left(\frac{N}{2}\right)^{-2}$ is the normalization factor to account for pairwise interaction between $\frac{N}{2}$ identical cations and anions. In prior work, our group has used

LD extensively to investigate charging processes in aerosols[73–78] and dusty plasmas.[79,80]

D. Calculation of electronic couplings

The coupling parameter $H_{if} = \frac{|E_1 - E_2|}{2}$ at $r = R_x$, where E_1 and E_2 are the energies of the two adiabatic states at the crossing point and can be calculated directly from the potential energy curves (PECs)—see Fig. 2(b). For small ion pairs such as $H^+ - H^-$ and $Li^+ - D^-$, a Full Configuration Interaction (FCI) method[81,82] may be used to obtain the PECs. However, to obtain the crossing point using the Nonadiabatic Coupling Matrix Elements (NACMEs) or the radial couplings, a reasonably well-resolved grid in the radial coordinate is required, which is used in the numerical finite difference method (DDR) procedure of MOLPRO. Because the DDR implementation in MOLPRO cannot be performed with FCI, all PECs in this study are calculated with the internally contracted multireference configuration interaction with single and double excitations (MRCISD). For all tested ion pairs, we used correlation consistent basis sets[83–85] and their variants such as aug-cc-pVQZ (AVQZ) and aug-cc-pwCVQZ (AWCVQZ). For lighter ions such as $H^+ - H^-, Li^+ - D^-, Ne^+ - Cl^-$, we tested additional larger basis sets, but for the heavier $Xe^+ - F^-$ pair we only tried the AVQZ basis set[85] due to computational resource limitations. The PEC computation for MN involves the highly excited product states A^* that result from the neutralization of the cation A^+. These excited states have energy levels lower than the ion dissociation limit such as the $Li(1s^2 3d^1)$ excited state. Consequently, larger basis sets are commonly needed to capture these high energy orbitals. All basis sets in this study are generated in MOLPRO by appending even-tempered functions to an existing basis set.[86]

III. RESULTS AND DISCUSSION: MONOATOMIC IONS

A. $H^+ - H^-$ ion pair

For $H^+ - H^-$, we calculated PECs for the seven lowest $^1\Sigma_g^+$ states and six lowest $^1\Sigma_u^+$ states. The PEC calculations were done for interatomic separation of $(1 - 50)a_0$ in increments of $0.1a_0$. The PECs and NACMEs are computed with MRCISD using a three-point central difference method with a step $\Delta r = 0.001a_0$ in MOLPRO. MOLPRO cannot handle non-Abelian point groups, so all homonuclear pairs will use the Abelian D_{2h} point group, with the following order of irreducible representations: $A_g, B_{3u}, B_{2u}, B_{1g}, B_{1u}, B_{2g}, B_{3g}, A_u$. A two electron/32 MO active space is used, with 9, 3, 3, 1, 9, 3, 3, 1 active MOs for the $^1\Sigma_g^+$ states, and 7, 3, 3, 1, 7, 3, 3, 1 active MOs for the $^1\Sigma_u^+$ states. Three basis sets were tested: (1) the augmented correlation consistent basis set aug-cc-pVQZ (AVQZ), (2) aug-cc-PV5Z (AV5Z) with four additional even-tempered function (ET4) to accurately capture the 3d orbitals, and (3) the basis set reported by Stenrup, Larson, and Elander[20] obtained by adding diffuse functions that are optimized for good representation of the hydrogen excited states to the original aug-cc-pVQZ basis set (AVQZ-ST). The atomic electronic excitation energies obtained with each basis set are compared to the experimental data from the NIST Basic Atomic Spectroscopy Database[87,88] in Table I.

The PECs computed at MRCISD level are similar to the PECs computed at FCI level by Stenrup, Larson, and Elander.[20] Among all the three basis sets used in this study, a globally maximum energy difference of less than 0.015 and 0.025 eV is observed for $^1\Sigma_g^+$ states and $^1\Sigma_u^+$ states, respectively. The PECs using AV5Z-ET4 are displayed in Fig. 4 (A: $^1\Sigma_g^+$ and B: $^1\Sigma_u^+$) and the PECs obtained using the other two basis sets showed no major differences and are not separately displayed. Figure 5 (A: $^1\Sigma_g^+$ and B: $^1\Sigma_u^+$) shows the computed NACMEs for n = 2 crossings using AVQZ-ET4 and AV5Z-ET4 basis sets against the *ab initio* quantum calculations of Stenrup, Larson, and Elander.[20] For clarity, calculations using all the tested basis sets are summarized by listing the radial location or crossing point R_x where the computed NACMEs reach maximum magnitude. The associated coupling values reported by Stenrup, Larson, and Elander[20] are shown in Tables II and III for n = 2 and n = 3 crossings. Tables S2-A and S2-B display the NACMEs corresponding to Tables II and III, respectively. As shown in Fig. 5, for the n = 2 crossing, all the tested basis sets are in good agreement with previously reported coupling values except for minor deviations in coupling between the second and third $^1\Sigma_g^+$ states and between the first and second $^1\Sigma_u^+$ states.

The computed nonadiabatic couplings are as expected, according to the appearance of the crossing points between the ionic (reactant) state curve and the neutral (product) state curves PECs. The couplings between the third and fourth $^1\Sigma_g^+$ states and between the second and third $^1\Sigma_u^+$ states are less significant compared to other couplings. The coupling between the second and fourth $^1\Sigma_g^+$ states and between the first and third $^1\Sigma_u^+$ states are the predominant pathways that connect the ionic state and the states associated with the covalent limit. It also shows a strong coupling between the two states associated with the covalent limit as expected from the shape of the PECs as well. However, for the n = 3 crossings only the couplings of the $^1\Sigma_g^+$ states are reported by Stenrup, Larson, and Elander.[20] So, for the $^1\Sigma_u^+$ states, the MOLPRO calculation with the reported AVQZ-ST basis set is used as the reference in this case. It is seen that calculations using all the basis sets show noticeable coupling between the fourth and seventh $^1\Sigma_g^+$ states, which connect the ionic and the covalent limit, but our current results show comparable couplings among all the states between fourth and seventh instead of

TABLE I. Energy levels of asymptotic atomic states for H – H (in eV).

Asymptotic atomic states	AVQZ-ET4	AV5Z-ET4	AVQZ-ET-S	NIST[88]
H(n = 1) + H(n = 1)	0	0	0	0
H(n = 1) + H(n = 2)	10.208	10.208	10.205	10.199
H(n = 1) + H(n = 3)	12.102	12.102	12.096	12.088

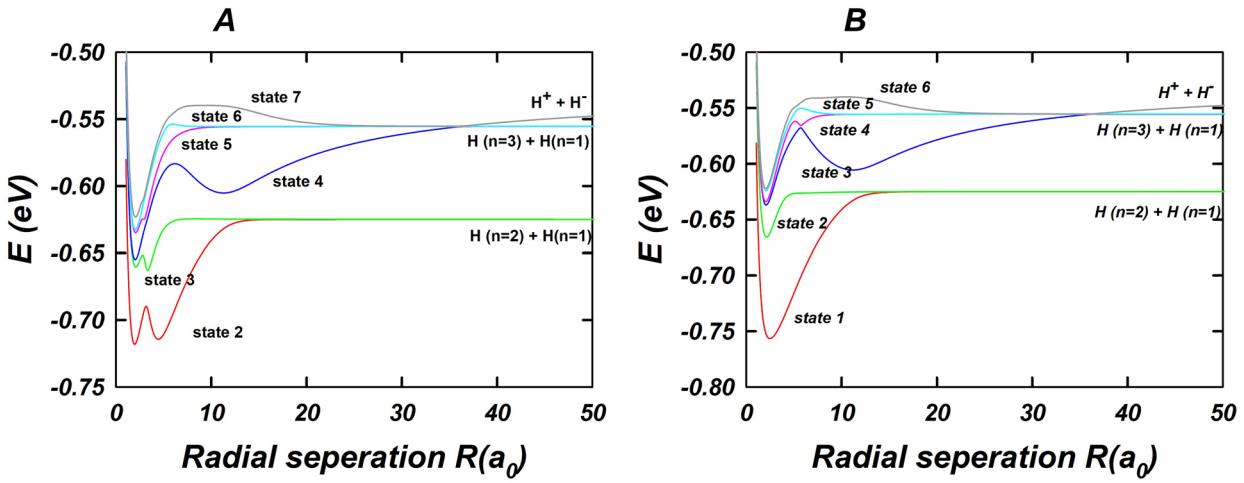

FIG. 4. (a) PECs of the second to seventh lowest $^1\Sigma_g^+$ states of H – H computed using the AVQZ-ET4 basis set in MOLPRO. Please refer to Table II for the location of crossings. (b) PECs of the six lowest $^1\Sigma_u^+$ states of H – H computed using the AVQZ-ET4 basis set in MOLPRO. Please refer to Table III for the location of crossings. The energy of State 1, the lowest-lying state that resembles the ground state of H_2 molecule, is not high enough to be directly accessible to the ionic state and is excluded from the PEC plot.

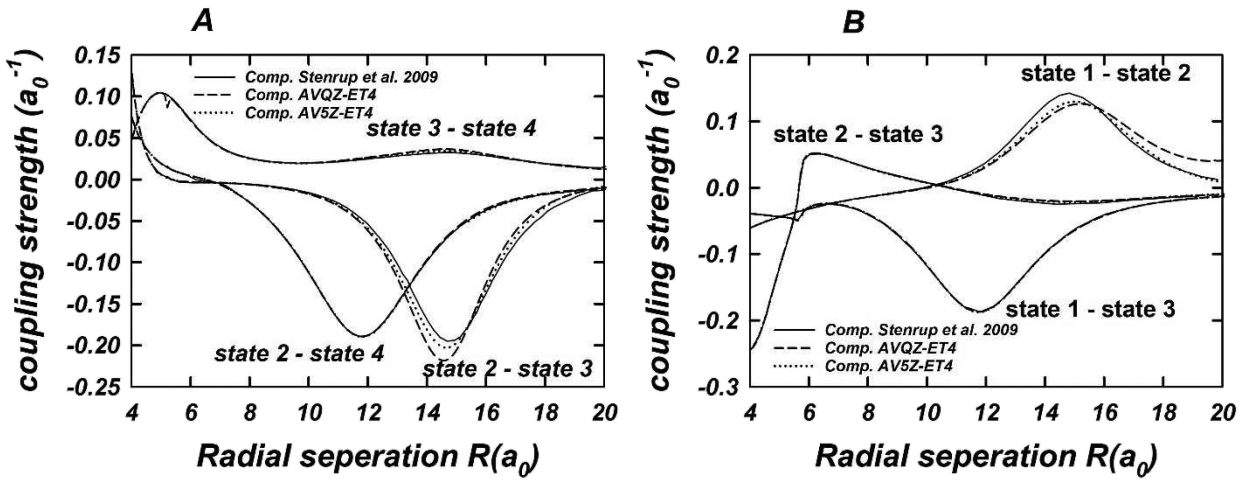

FIG. 5. (a) NACMEs of $^1\Sigma_g^+$ n = 2 crossings computed using the AVQZ-ET4 and AV5Z-ET4 basis sets in MOLPRO and compared with the calculations reported by Stenrup, Larson, and Elander.[20] Please refer to Table S2-A, for NACME values. (b) NACMEs of $^1\Sigma_u^+$ n = 2 crossings computed using the AVQZ-ET4 and AV5Z-ET4 basis sets in MOLPRO and compared with the calculations reported by Stenrup, Larson, and Elander.[20] Please refer to Table S2-B for NACME values.

a distinct coupling between the fourth and the seventh states. This might be due to our selection of active space that had an insufficient number of higher orbitals or a non-optimal basis set and requires some future reexamination. For the current study, we deem these calculations to be accurate enough for electron transfer probability p_{LZ} estimation using Eq. (2) and subsequent incorporation into trajectory simulations.

The speed-dependent cross section $\sigma(v)$ for H – H in free-molecular limit is computed using the R_x, H_{12} for the crossings incorporated into the MC trajectory simulations as described earlier. We carried another set of MC trajectory calculations of $\sigma(v)$ with R_x, H_{12} inputs from Olson, Peterson, and Moseley.[27] The cross section is evaluated under the two limits of no and instant de-excitation. The former treatment is equivalent to Olson's method of cross section evaluation. At the other limit, the de-excitation rate is artificially set to infinity (instantaneous de-excitation) so a single adiabatic transition will lead to an effective neutralization, wherein any excited species formed are instantly reduced to their

TABLE II. R_x of H – H $^1\Sigma_g^+$ states with all tested basis sets (in atomic units).

$R_x(a_0)$	AVQZ-ET4	AV5Z-ET4	AVQZ-ET-S	Stenrup, Larson, and Elander[20]
n = 2, state 2–3	14.5	14.6	14.7	14.8
n = 2, state 2–4	11.8	11.8	11.8	11.7
n = 2, state 3–4	14.6	14.5	14.7	14.5
n = 3, state 4–5	36.0	36.7	37.0	36.9
n = 3, state 4–6	36.0	36.1	36.2	36.1
n = 3, state 4–7	36.0	36.1	35.9	35.9
n = 3, state 5–6	35.9	35.9	36.5	36.5
n = 3, state 5–7	36.1	36.4	35.8	35.8
n = 3, state 6–7	36.2	36.3	35.5	35.5

TABLE III. $R_x(a_0)$ of H – H $^1\Sigma_u^+$ states with all tested basis sets (in atomic units).

$R_x(a_0)$	AVQZ-ET4	AV5Z-ET4	AVQZ-ET-S	Stenrup, Larson, and Elander[20]
n = 2, state 2–3	15.1	15.0	14.8	14.8
n = 2, state 2–4	11.7	11.7	11.7	11.8
n = 2, state 3–4	15.0	14.9	14.7	14.4
n = 3, state 4–5	36.0	36.7	36.7	⋯
n = 3, state 4–6	36.0	36.1	36.1	⋯
n = 3, state 4–7	36.0	36.1	35.9	⋯
n = 3, state 5–6	35.9	36.0	36.3	⋯
n = 3, state 5–7	36.1	36.4	35.8	⋯
n = 3, state 6–7	36.2	36.3	35.5	⋯

respective ground states and any possibility for re-ionization is prohibited because ground state energies are often too low to intersect an ionic state curve. The cross sections using each tested basis set at each of the two de-excitation limits are shown in Fig. 6 along with experimental data. The cross section at the instant de-excitation limit is higher than the corresponding value where the de-excitation is prohibited. Differently from the classical treatment used in this study and that of Olson, Peterson, and Moseley,[27] Stenrup, Larson, and Elander[20] have evaluated the cross section using a molecular close-coupling approach with all degrees of freedom treated quantum mechanically. The $\sigma(v)$ obtained using this approach are ~15% higher than cross sections calculated by Olson, Peterson, and Moseley[27] for low energy thermal collisions. The cross section values obtained in the current study using the optimized basis set by Stenrup, Larson, and Elander[20] are close to those obtained by Olson, Peterson, and Moseley[27] at low collision energies. The highlight of the current approach is the semiclassical treatment of electron transfer using LZ theory and coupling it with trajectory simulations to capture the effect of gas pressure with scope for incorporating additional physics such as external electric or magnetic fields, de-excitation through collisions with neutrals, and/or by photon emission. The cross sections using even-tempered aug-cc-pVQZ and aug-cc-pV5Z basis sets are almost identical but are somewhat larger than the full quantum result reported by Stenrup, Larson, and Elander.[20] When the instantaneous de-excitation assumption is utilized, surprisingly, the cross sections are closer to the experimental values reported by Moseley, Aberth, and Peterson[23] and Rundel,

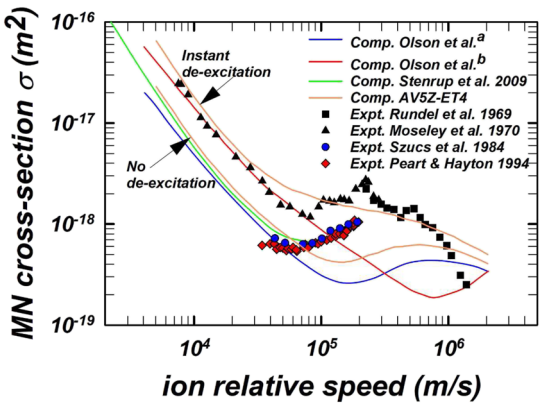

FIG. 6. H – H MN cross section $\sigma(v)$. Experimental data ("Expt.") reported by Rundel, Aitken, and Harrison,[24] Moseley, Aberth, and Peterson,[23] Szucs, Karemera, Terao, and Brouillard,[22] and Peart and Hayton[21] are plotted. Computations ("Comp.") reported by Olson, Peterson, and Moseley[27] computed using two parameterizations: H^a_{if} developed by Olson, Smith, and Bauer[48] denoted as *Olson et al.*.[a] and H^b_{if} denoted as *Olson et al.*.[b] The *ab initio* calculations of Stenrup, Larson, and Elander[20] and the MC trajectory simulation calculations of the current study using the AV5Z-ET4 basis set are also reported. MC calculations using the AVQZ-ET4 basis set are indistinguishable from the AV5Z-ET4 results and are not plotted here. The calculations using AVQZ-ST are similar to that of the AV5Z-ET4 results at low energy collisions and show only minor differences at higher energies and are also not displayed for clarity. Finally, the calculations presented here are for the $^1\Sigma_g^+$ state; the results for $^1\Sigma_u^+$ are nominally identical and are not shown.

Aitken, and Harrison.[24] We think that the de-excitation times of specific ions must be used to judge the validity of the cross section using the instant de-excitation assumption.

B. $Li^+ - H^-$ ion pair

For $Li^+ - H^-$, we computed the six lowest $^1\Sigma^+$ states up to the crossing associated with the Li (3d) excited state. Since the next excited state of Li (4p) is expected to have a crossing distance >200a_0, at such distances the LZ transition is expected to be negligible.[27] The PEC calculations were done for interatomic separations from 2a_0 to 50a_0 in increments of 0.1a_0. Heteronuclear pairs are described in MOLPRO using Abelian C_{2v} point group symmetry with the following ordering of irreducible representations: A_1, B_1, B_2, A_2. The active space used in the calculation is four electron/16 MO, with 9, 3, 3, 1 active MOs. Three basis sets were tested: the augmented correlation consistent basis set aug-cc-pVQZ (AVQZ), aug-cc-pV5Z (AV5Z) with two additional even-tempered (-ET2) function on Li to accurately capture the 3d orbitals, and an aug-cc-pwCVQZ (AWCVQZ) basis set with only one even-tempered diffuse function (-ET1) on Li. For all runs, the basis set for H was kept as AV5Z that accurately reproduces the electron affinity of H. The asymptotic energy level of each state obtained with each of the basis sets used is reported in Table IV along with corresponding experimental data from the NIST Basic Atomic Spectroscopy Database.[87–90] The PECs computed at MRCISD level are comparable to those computed at the FCI level reported in the work of Launoy *et al.*[91] using a modified version of aug-cc-pCV5Z, referred to as ACV5Z + G. The NACMEs are evaluated using the DDR program in MOLPRO using a three-point central difference method in step $\Delta r = 0.001a_0$. The positions of the crossings computed using each basis set and the corresponding values reported in the work of Launoy *et al.*[91] are shown in Table V; the corresponding nonadiabatic couplings are displayed in Table S2-C.

All computed crossing distances in this study are smaller than the values reported in the work of Launoy *et al.*[91] by no more than 0.4a_0. The computed nonadiabatic couplings are also comparable to the results reported in the work of Launoy *et al.*[91] except for the AWCVQZ basis set at the crossing between Li (3d) excited state and the ionic state, even though this basis set yields the most accurate excitation energies with respect to the spectroscopy data. For all tested basis sets, the computed NACMEs between each consecutive state have discernible values at the distances where a crossing is expected according to the PECs shown in Fig. 7(a). All couplings have distinguishable peaks, especially for the two couplings between the fourth and fifth states at 33.8a_0 and between the fifth and sixth states at 35.5a_0 where the associated states have similar energies that result in similar crossing distances. For these two crossings sharp individual peaks are observed. Therefore, Li – H is an ideal chemical system for the application of LZ theory. A plot of the couplings obtained with AVQZ-ET2 is shown in Fig. 7(b). The absolute values of nonadiabatic couplings are used since the sign of the couplings changes due to the phase change of the wave functions in MOLPRO.

TABLE V. R_x of Li – H with all tested basis sets (in atomic units).

$R_x(a_0)$	AVQZ-ET2	AV5Z-ET2	AWCVQZ-ET1	Launoy *et al.*[91]
State 1–2	6.90	6.90	6.80	7.20
State 2–3	11.00	11.20	11.00	11.30
State 3–4	22.00	22.00	21.90	22.05
State 4–5	33.80	33.70	33.50	34.40
State 5–6	35.50	35.50	35.70	35.90

Figure 8 shows the MN cross section $\sigma(v)$ obtained using noted basis sets, the *ab initio* calculations used in the work of Launoy *et al.*[91] using the ACV5Z + G basis set and using the ET-Li basis set developed by Gim and Lee,[92] along with experimental data. The small deviation in the quantum chemistry results does not have a noticeable impact on the cross section calculation and all test basis sets yield nearly identical cross sections. Across the entire range of collision energy or relative speed, our result agrees very well with the cross section computed in the work of Launoy *et al.*[91] where the basis set used was ACV5Z + G. Therefore, similar to the result reported in the work of Launoy *et al.*,[91] our simulation agrees well with the experiments for low energy collisions but has some disagreements for high energy collisions. As reported in the work of Launoy *et al.*,[91] none of the basis sets tested show a strong influence on the cross section calculation at low collision energies. Discrepancies start to appear when the collision energy becomes high, at which relativistic effects may be significant and the Born–Oppenheimer approximation used to simplify quantum calculations may reduce accuracy. Interestingly, the corresponding ET-Li basis set used by Gim and Lee[92] shows a clear difference from the ACV5Z + G result across the entire collision energy range. The result where the de-excitation is assumed to be instantaneous is higher than the no de-excitation limit as expected and again shall only be considered as an estimation of the fast de-excitation limit even though it is not a physically plausible scenario. The results of the two de-excitation limits appear to be nearly parallel for the velocity range chosen. For the collision energy range of Peart and Hayton,[21] our simulation results indicate

TABLE IV. Energy levels of Li – H asymptotic atomic states for tested basis sets (in eV).

Asymptotic atomic states	AVQZ-ET2	AV5Z-ET2	AWCVQZ-ET1	NIST[109]
Li (2s) + H(1s)	0	0	0	0
Li (2p) + H(1s)	1.835	1.837	1.848	1.848
Li (3s) + H(1s)	3.361	3.366	3.376	3.373
Li (3p) + H(1s)	3.816	3.821	3.833	3.834
Li (3d) + H(1s)	3.857	3.864	3.883	3.879

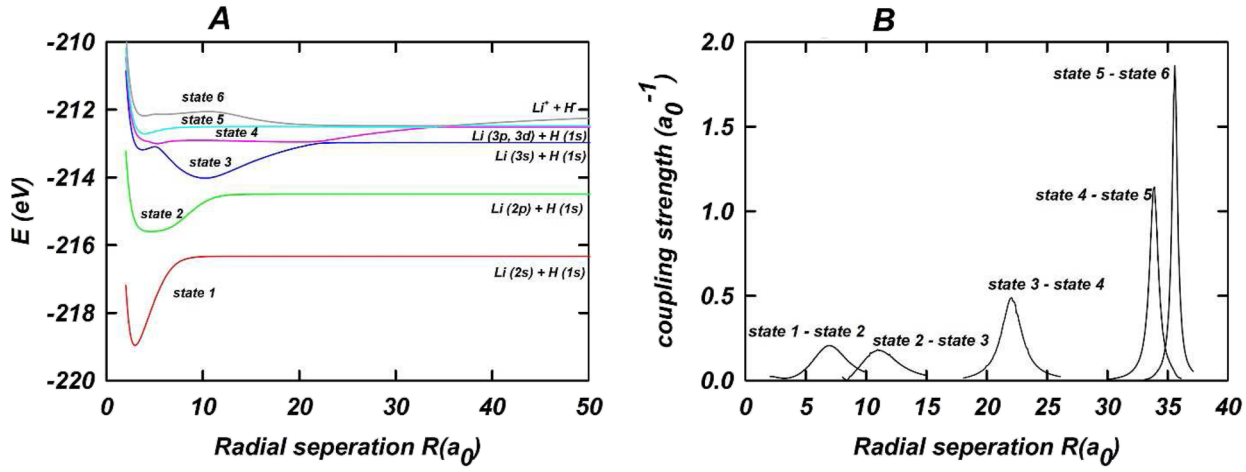

FIG. 7. (a) PECs of Li – H using AVQZ-ET2 basis set in MOLPRO. (b) NACMEs of Li – H using AVQZ-ET2 basis set in MOLPRO.

that the third and fourth crossings are predominant for intermediate collision energies, and the second, third, and fourth crossings have noticeable contribution to the final product. The third crossing contributes 65%–77% to the final product across the range, where this crossing will lead to a product of Li (3s). We do not expect the result of MRCISD and FCI to have significant differences for the current four-electron system of $Li^+ - H^-$. Another expected source of error is the classical trajectory treatment of the LZ theory itself even if the nonadiabatic coupling values at each crossing can be approximated as a two state crossing. It is shown by Stenrup, Larson, and Elander[20]

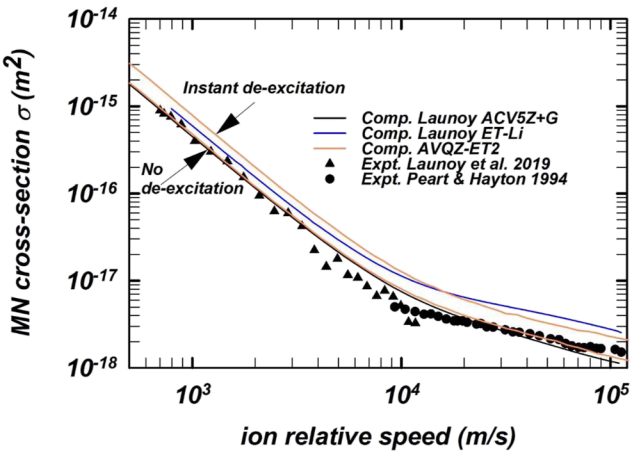

FIG. 8. Li – H MN cross section $\sigma(v)$. Experimental data ("Expt.") reported in the work of Peart and Hayton[21] and Launoy *et al.*[91] are plotted. Computations ("Comp.") reported in the work of Launoy *et al.*[91] computed using two basis sets ACV5Z + G and ET-Li are plotted. The MC trajectory simulation calculations of the current study using the AVQZ-ET2 basis set is also reported. MC calculations using the AV5Z-ET2 and AWCVQZ-ET1 basis sets are indistinguishable from the AVQZ-ET2 results and are not plotted here. Finally, the calculations presented here are for the $^1\Sigma^+$ state.

that a full-quantum calculation can lead to a large difference in cross section. As a future study, a full-quantum calculation may be developed for the Li – H ion pair, especially for higher energy collisions to obtain benchmarking data.

It is shown experimentally across the range of collision energies from 3.9 to 200 meV, corresponding to speeds from 700 to 5000 m/s, the branching ratios are insensitive to the collision speed. In our runs, N_{neu} is increased to 100 000 for higher statistical accuracy, and the obtained branching ratios are shown in Table VI. The branching ratio obtained using our MC simulation qualitatively agrees with the experiment with a branching ratio >50% for the product channel of Li (3s). In contrast with the ACV5Z + G basis used in the work of Launoy *et al.*[91] where the additional diffuse function is optimized, the even-tempered basis sets used in this study yield a slightly higher ratio at the Li (3d) channel and a slightly lower ratio at the Li (3s) channel. For the runs where instant de-excitation is assumed, a branching ratio of ~20% is observed at the Li (2p) channel. However, instant de-excitation is not a physically plausible model, especially in the free-molecular limit. In the future, incorporation of unimolecular de-excitation physics through transition rules could potentially improve the accuracy of our calculations.

C. MN of rare gas cations and halide anions

The effect of gas pressure on the MN reaction between a rare gas cation R^+ reacting with halide anion X^- is not fully quantified, even though such reactions are of fundamental interest in the study of ionized gas clouds in interstellar space, planetary ionospheres, and energy systems, and are amenable to be treated using the LZ approach due to the long-range attraction and electron transfer crossings found outside the range of van der Waals potential. Experimental studies of this type of reaction are sparse and the free-molecular limit rates, usually estimated based on LZ model, are used at finite low pressures as well since the extrapolation of experimental data from the high-pressure limit introduces considerable amounts of uncertainty. In the current work, we examine two $R^+ - X^-$ pairs

TABLE VI. Branching fraction (%) of Li − H using each basis set along with experimental and computational results from the work of Launoy *et al.*[91]

			Li (2*s*)	Li (2*p*)	Li (3*s*)	Li (3*p*)	Li (3*d*)	Li (4*s*)
Experimental (Expt.) and computational (comp.) results by Launoy *et al.*[91]		Expt. 3.9 meV			63.4	26.6	10.0	
		Expt. 20 meV			60.0	32.0	8.0	
		Expt. 200 meV			59.9	33.7	6.5	
		Comp. ACV5Z + G	0	0	60.1	30.5	8.9	0.5
		Comp. ACV5Z	0	0	15.5	75.0	9.1	0.4
		Comp. ET_mid	0.3	24.4	52.2	17.5	5.1	0.5
		Comp. ET_Li	0	0	11.8	42.0	45.8	0.3
		Croft, Dickinson, and Gadéa[110]			66	31	3	
This study: No de-excitation limit	3.9 meV	AVQZ-ET2	0.0	0.0	53.5	32.9	13.6	⋯
		AV5Z-ET2	0.0	0.0	52.5	34.3	13.2	⋯
		AWCVQZ-ET1	0.0	0.0	57.9	40.1	2.0	⋯
	20 meV	AVQZ-ET2	0.0	0.0	53.4	33.1	13.6	⋯
		AV5Z-ET2	0.0	0.0	53.0	33.9	13.2	⋯
		AWCVQZ-ET1	0.0	0.0	57.8	40.3	2.0	⋯
	200 meV	AVQZ-ET2	0.0	0.0	54.3	32.5	13.2	⋯
		AV5Z-ET2	0.0	0.0	53.6	33.4	12.9	⋯
		AWCVQZ-ET1	0.0	0.0	59.0	39.0	2.0	⋯
This study: Instant de-excitation limit	3.9 meV	AVQZ-ET2	0.0	18.0	55.8	18.8	7.5	⋯
		AV5Z-ET2	0.0	18.1	55.3	19.3	7.3	⋯
		AWCVQZ-ET1	0.0	18.1	59.3	21.5	1.1	⋯
	20 meV	AVQZ-ET2	0.0	17.8	55.8	18.7	7.7	⋯
		AV5Z-ET2	0.0	17.9	55.2	19.6	7.3	⋯
		AWCVQZ-ET1	0.0	18.1	59.2	21.7	1.0	⋯
	200 meV	AVQZ-ET2	0.0	17.9	55.4	19.1	7.6	⋯
		AV5Z-ET2	0.0	18.0	55.0	19.7	7.4	⋯
		AWCVQZ-ET1	0.0	18.2	59.1	21.7	1.0	⋯

with limited level of accuracy in our quantum calculations and compute their MN rate constant β. Specifically, a preliminary modeling study of $Ne^+ - Cl^-$ in the low-pressure limit (~1 Torr) and $Xe^+ - F^-$ in the high-pressure limit ($\sim 10^4$ Pa) is conducted. Experimental data from the work of Shuman *et al.*[15] and Lee and Johnsen[61] pertaining to these two reactions, respectively, are used for assessing the physical validity of our approach.

Olson[27,44,53] applied the LZ transition state theory in free-molecular or zero pressure limit. The critical input to the theory, namely, the adiabatic electronic coupling H_{if}, was evaluated using an empirical fit[48] that only qualitatively describes the relationship between H_{if} and the crossing distance R_x, the binding energy of the anion EA. This fit is useful for estimating the cross section and rate constant for one electron transfer reactions involving hydrogen-like species. However, a case-specific H_{if} coming from quantum chemistry computation is still preferred, if possible since the cross section is a nontrivial function of individual crossings. Moreover, outcomes at a crossing affects the probability sequences for other crossings. In other words, even though MN reactions involving single electron transfer are of interest, it is not ideal to use a $H_{if}(R_x)$ fit developed by analyzing experimental data and *ab initio* calculations for hydrogen-like species for large, multi-electron systems such as $R^+ - X^-$ or polyatomic species. We will show shortly below that the rate constants computed using trajectory simulations are not extremely sensitive to the accuracy level of the quantum calculations, and MRCISD calculations still allow us to elicit reasonable predictions that compare well with observations.

D. $Ne^+ - Cl^-$ ion pair

To examine the MN reaction at low pressure, $Ne^+ - Cl^-$ ion pair was chosen primarily because there exists experimental data reported in the work of Shuman *et al.*[15] for validation. Among the 12 $R^+ - X^-$ combinations experimentally characterized, the $Ne^+ - Cl^-$ pair has the least number of electrons, and the spin–orbit coupling is significantly less compared with heavier atoms in the matrix. Another technical difficulty related to the quantum calculation is that the ionization limit of Cl (13.0 eV) falls below the first excited state of Ne (16.2 eV). Consequently, to obtain an accurate description of the crossing channels associated with Ne (3s), an expanded set of orbitals needs to be included in the active space to account for the excited states of Cl. This is computationally prohibitive for the MRCISD method. In this study, the active space is chosen as 10, 4, 4, 0, which is obtained by appending 2, 1, 1, 0 to the valence

orbitals to capture the 3s orbital of Ne while still being computationally tractable. The active space is indexed following the irreducible representation in MOLPRO for C_{2v} point group. The alternative solution utilized in the current study is manually choosing a configuration set that is expected to be important for the excited states of Ne as well as the ionic state of two ions. This results in a total of 8 configurations corresponding to 14 Configuration State Functions (CSFs) used to solve for the six lowest $^2\Sigma^+$ states where all product states that dissociate into an excited state of Cl are excluded. A total of 13 configurations corresponding to 26 CSFs are used to solve for the six lowest $^2\Pi^+$ states. MOLPRO also provides a "RESTRICT" option, which can be used to exclude a certain pattern of electron occupation. However, while invoking the "RESTRICT" option, the resulting orbitals become highly unpredictable and may fail to capture the desired states. Manually inputting the configurations is certainly not an ideal solution to this situation, and the process of selecting an active space needs to be further refined in the future, especially with regard to obtaining desired product states. The basis sets are chosen to be the aug-cc-pwCVQZ (AWCVQZ) and aug-cc-pwCV5Z (AWCV5Z) with two even-tempered function on the s, p, d, and f orbitals (-ET2) for both Ne and Cl. The energy differences at the covalent limit computed are reasonable compared with the excitation energy for Ne measured in spectroscopy experiments, and the crossing distances are reasonable judging from the appearance of the PECs. For the non-FCI method, size consistency is not guaranteed and usually, the Davidson correction[93,94] is included as a correction for triple excitation. However, for the current case since the configuration is selected manually, the Davidson correction does not return reasonable PECs and for all computations the MRCISD energies are used. The energy level of each covalent limit obtained by each basis set and under each symmetry is listed in Table VII along with corresponding experimental data from the NIST Basic Atomic Spectroscopy Database.[48,87,95–97] The PECs for the second to sixth $^2\Sigma^+$ and $^2\Pi^+$ states are computed for reaction coordinate $(4-25)a_0$ in steps of $0.5a_0$, and near the crossing points a finer resolution of $0.1a_0$ is used; the corresponding PECs are shown in Fig. 9 (A: $^2\Sigma^+$ and B: $^2\Pi^+$). As for the smaller ion pairs, the DDR program is utilized to evaluate the nonadiabatic couplings with a three-point method with $\Delta r = 0.001a_0$.

For the $^2\Sigma^+$ states, both the tested basis sets show abnormal strong couplings around $14.3a_0$ and $14.5a_0$, whereas from the PEC it is apparent that at these distances the third and fourth states become almost degenerate. This spurious coupling is suspected to be due to defects in the selection of configurations. The second and fourth states are associated with $Ne\,2p^5\left(^2P_{\frac{3}{2}}\right)3s^1$ excited states, and are as expected, smoothly coupled and peak at $14.8a_0$ (according to calculations using the AWCVQZ-ET2 basis set) and at $14.9a_0$ (while using the AWCV5Z-ET2 basis set). The nearly same location where the peak coupling is found using both basis sets conforms well with the appearance of the PEC. For the second sets of crossings, noticeable couplings between the fourth and sixth states and the fourth and fifth states are observed while the coupling between the fifth and sixth states is negligible. For the $^2\Pi^+$ states, the couplings between

TABLE VII. Energy levels (in eV) of Ne − Cl asymptotic states for tested basis sets.

Asymptotic atomic states	AWCVQZ-ET2, Σ	AWCV5Z-ET2, Σ	AWCVQZ-ET2, Π	AWCV5Z-ET2, Π	NIST[95,96]
$Ne(2p^6) + Cl(3p^5)$	0	0	0[a]	0[a]	0.11
$Ne(2p^5\,3s^1) + Cl(3p^5)$	16.13	16.15	15.97	16.16	16.62

[a]In this study, the ground states of $^2\Sigma^+$ and $^2\Pi^+$ were taken as the reference for each symmetry, two symmetries are treated separately due to the manually input configuration set.

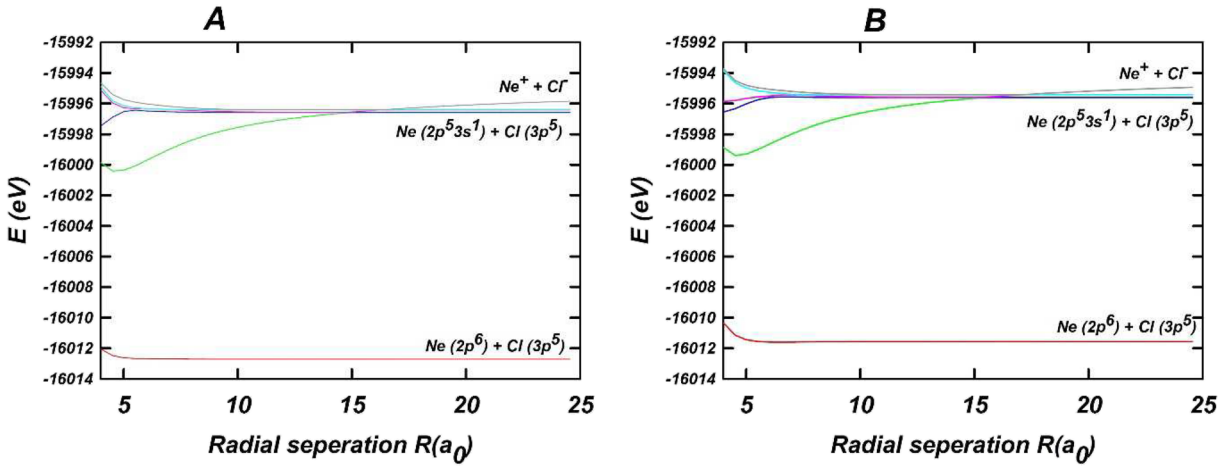

FIG. 9. (a) PECs of the six lowest Ne − Cl $^2\Sigma^+$ states computed using AWCVQZ-ET2 basis set in MOLPRO. (b) PECs of the six lowest Ne − Cl $^2\Pi^+$ states computed using AWCVQZ-ET2 basis set in MOLPRO.

TABLE VIII. Ne – Cl MN rate constant $\left(\times 10^{-14}\,\frac{m^3}{s}\right)$ obtained with tested basis sets.

De-excitation limit	AWCVQZ-ET2, Σ	AWCV5Z-ET2, Σ	AWCVQZ-ET2, Π	AWCV5Z-ET2, Π	Hickman[51]	Shuman *et al.*[15]
No de-excitation	8.91	8.74	6.87	6.70	8.83	3.0 ± 1.1
Instant de-excitation	11.68	10.99	8.71	8.16	⋯	⋯

the states associated with covalent limits are very less pronounced compared to the couplings between state 2 and 4 as well as state 4 and 6. For the $^2\Sigma^+$ states, we obtained an energy difference of nearly 0.17 eV between the two covalent limits for both AWCVQZ + 2 and AWCV5Z + 2 due to mainly different spin configurations of Ne, and for the $^2\Pi^+$ states the energy difference is 0.18 eV. Finally, Table VIII displays the MN rate constant β obtained by LD trajectory simulation using electron transfer probabilities computed using the AWCVQZ-ET2 and AWCV5Z-ET2 basis sets along with the prediction of a rate constant fit by Hickman.[51] Interestingly, Hickman[51] derives a generalization of the ASM and invokes the LZ theory to describe transitions in which the energy levels of the products are treated as a quasi-continuum to obtain a probability of electron transfer in a MN reaction analogous to Eq. (2) but one that depends only on the angular momentum quantum number l. Various approximations notwithstanding, both Hickman's fit and the current method led to an overestimation of the rate constant by approximately a factor of ~3 and ~2.5, respectively, when compared to the experimentally obtained $Ne^+ - Cl^-$ MN rate constant of $3.0 \pm 1.1 \times 10^{-14}\,\frac{m^3}{s}$.

E. $Xe^+ - F^-$ ion pair

The MN reaction rate constant of $Xe^+ - F^-$ ion pair in *He* background gas has been measured by Lee and Johnsen[61] from 20 000 to 80 000 Pa. At such pressures, the effect of ion-neutral interactions is expected to be dominant and the rate constant scales linearly with pressure.[98,99] Before presenting the comparisons between our rate constant calculations and measurements, we discuss PEC calculations for the Xe – F system. For this specific ion pair, the covalent limits are easy to determine since the ionization energy of Xe is lower than the first excitation energy of F. The only permissible crossings are the ones associated with the ionic state and $Xe\,5p^5\left(^2P_{\frac{3}{2}}\right)6s^1$ excited state. No crossings associated with the $Xe\,5p^5\left(^2P_{\frac{1}{2}}\right)6s^1$ limit should be observed in the result. The experimental values for each energy level is taken from the NIST basic atomic spectroscopy database.[87,100–104] For heavier elements such as xenon, relativistic effects become more significant and the splitting of energy levels due to spin–orbit coupling cannot be neglected. It was reported that spin–orbit coupling can be included by using a four-component approach based on the Dirac Hamiltonian, and this method can lead to satisfactory results for splitting within 15% of experimental values.[105] Unfortunately, this methodology is not included in MOLPRO and the values obtained in this study used MRCISD with spin–orbit coupling calculated based on the Breit–Pauli operator or spin–orbit pseudopotential.[106] The active space currently used is 11, 5, 5, 1, which is obtained by appending 2, 1, 1, 0 orbitals to the valence orbitals. The orbitals are indexed the order of A_1, B_1, B_2, A_2 under C_{2v} point group. With this choice of active space, around

TABLE IX. Energy levels (in eV) of Xe – F asymptotic atomic states.

Asymptotic atomic state	Molecular state	AVQZ	NIST[103,104]
$Xe(5p^6) + F\left(2p^5, {}^2P_{\frac{3}{2}}\right)$	$^2\Pi^+$	0	0
$Xe\left(5p^5 6s^1, {}^2[3/2]_2\right) + F\left(2p^5, {}^2P_{\frac{1}{2}}\right)$	$^2\Pi^+$	8.22	8.37
$Xe\left(5p^5 6s^1, {}^2[3/2]_1\right) + F\left(2p^5, {}^2P_{\frac{1}{2}}\right)$	$^2\Pi^+$	8.27	8.49
$Xe\left(5p^5 6s^1, {}^2[1/2]_0\right) + F\left(2p^5, P_{\frac{3}{2}}\right)$	$^2\Pi^+$	8.56	9.45
$Xe\left(5p^5 6s^1, {}^2[1/2]_1\right) + F\left(2p^5, {}^2P_{\frac{3}{2}}\right)$	$^2\Pi^+$	8.95	9.57
$Xe^+\left(5p^5, {}^2P_{\frac{3}{2}}\right) + F^-\left(2p^6\right)$	$^2\Pi^+$	⋯	8.73
$Xe\left(5p^6\right) + F\left(2p^5, {}^2P_{\frac{1}{2}}\right)$	$^2\Sigma^+$	−0.01	0.05
$Xe\left(5p^5 6s^1, {}^2[3/2]_2\right) + F\left(2p^5, {}^2P_{\frac{3}{2}}\right)$	$^2\Sigma^+$	8.37	8.32
$Xe\left(5p^5 6s^1, {}^2[3/2]_1\right) + F\left(2p^5, P_{\frac{3}{2}}\right)$	$^2\Sigma^+$	8.47	8.44
$Xe\left(5p^5 6s^1, {}^2[1/2]_0\right) + F\left(2p^5, {}^2P_{\frac{1}{2}}\right)$	$^2\Sigma^+$	9.43	9.50
$Xe\left(5p^5 6s^1, {}^2[1/2]_1\right) + F\left(2p^5, {}^2P_{\frac{1}{2}}\right)$	$^2\Sigma^+$	9.54	9.62
$Xe^+\left(5p^5, {}^2P_{\frac{1}{2}}\right) + F^-\left(2p^6\right)$	$^2\Sigma^+$	⋯	9.99

47 000 CSFs are used in each MCSCF calculation for each symmetry and the following MRCISD is computed with a configuration selection threshold of 0.04 to the norm of all CSFs to limit computational times. Calculations are performed using aug-cc-pVQZ (AVQZ) basis set for both Xe and F. A pseudo-potential (-PP) ECP28MDF[85] is used for Xe where 28 core electrons are parametrically represented. Computed energy levels of each covalent limit are shown in Table IX.

Since the spin–orbit coupling cannot be incorporated into the DDR program within MOLPRO, the crossing points for the $Xe^+ - F^-$ ion pair are determined by computing the energy difference between states and the points corresponding to the minimum energy difference are taken as the crossing points in the PECs shown in Fig. 10 (A: $^2\Sigma^+$ and B: $^2\Pi^+$). The energy of the $Xe\left(5p^5 6s^1, {}^2[1/2]_0\right) + F\left(2p^5, {}^2P_{\frac{3}{2}}\right)$ and $Xe\left(5p^5 6s^1, {}^2[1/2]_0\right) + F\left(2p^5, {}^2P_{\frac{3}{2}}\right)$ asymptotic atomic limit are noticeably lower (see Table IX) than the NIST atomic spectroscopy data than for any of the other crossings. A crossing is seen for these states based on the current calculations, but based on only NIST data, a crossing would not be expected. These spurious crossings are suspected to be due to misidentifying molecular states from spin–orbit coupling results. So, the crossings associated with these two states are not included in the trajectory simulations. In addition, the ion dissociation limit for the $^2\Sigma^+$ molecular state is higher in energy than the ground ionic state by 1.26 eV. So, we considered only the transitions between the $^2\Pi^+$ states.

The MN rate constants from simulation in the pressure range of ~20 000 to 80 000 Pa show insignificant dependency on the actual electronic coupling values. The increased pressure premises the formation of pseudo-stable elliptical orbits that are terminated using the energy criterion of Eq. (8). Orbit formation allows the ions to pass the LZ crossing (at least corresponding to the lowest or closest crossing) at a high frequency, which increases the effective probability of electron transfer. The pressure effect determines the lower limit of the reaction rate, which is equal of the rate of orbit formation

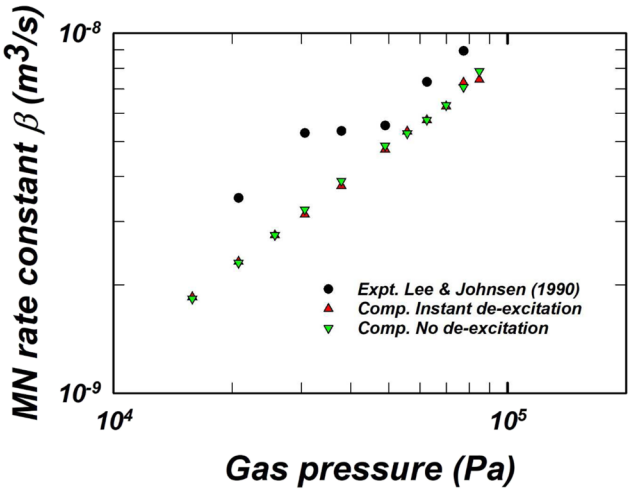

FIG. 11. Xe – F MN rate constant $\beta(p_g)$ $\sigma(v)$. Experimental data ("Expt.") reported by Lee and Johnsen[61] are plotted along with LD trajectory simulation calculations ("Comp.") of the current study for Xe – F $^2\Pi^+$ states.

in the current case since the very weak couplings associated with LZ type electron transfer cannot result in a larger cross section that overcomes orbit formation rate. Simulation results also show reasonable agreement with experimental data as well as a near-linear dependency of pressure as shown in Fig. 11. The circles are the measurements reported by Lee and Johnsen,[61] and the upward and downward triangles are the values obtained by simulation in this study at each de-excitation limit. Reasonable agreement is seen between measurement and prediction, with the predictions being within a factor of 3 for the pressure range considered.

Another source of error in our LD simulations at high pressures is expected to be the near-range electron transfer when the ions

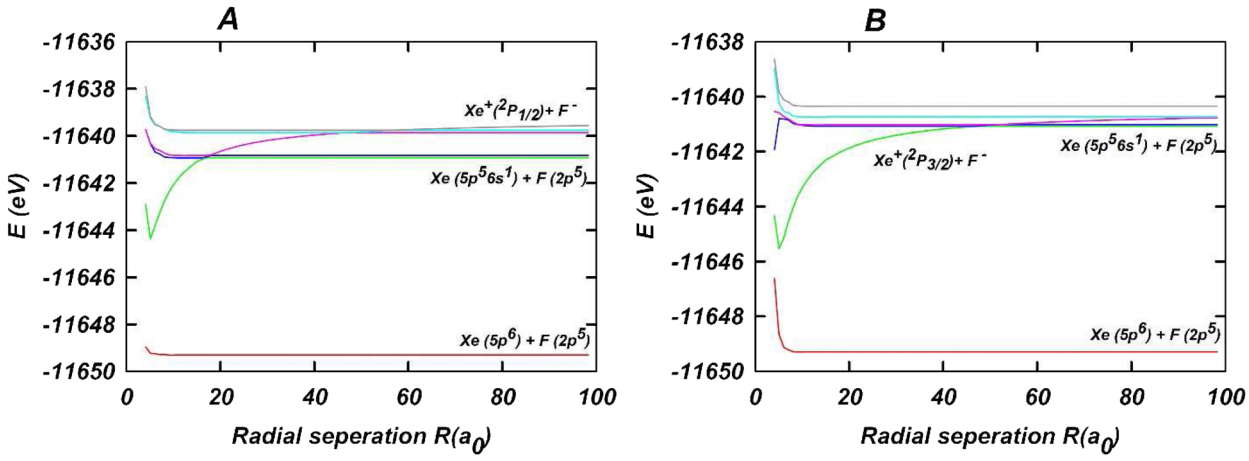

FIG. 10. (a)PECs of the six lowest Xe – F $^2\Sigma^+$ states computed using AVQZ-PP basis set in MOLPRO. (b) PECs of the six lowest Xe – F $^2\Pi^+$ states computed using AVQZ-PP basis set in MOLPRO.

get close enough to each other where the Lennard-Jones potential becomes effective. More discussion and a full-scale *ab initio* molecular dynamics simulation is needed to study the details of this type of short-range electron transfer and is a subject for future work. In the current study, we have focused on long-range electron transfer that is driven by Coulombic interactions well outside the range of the Lennard-Jones potential between the ions. This scenario is well described by the LZ theory, and we have coupled the same to classical trajectory simulations to build a robust approach to capture the effect of gas pressure on MN reactions. In the current study, the Lennard-Jones parameters intended to describe the ground state of atoms are used. In the future investigations, it could be better to use corresponding Lennard-Jones parameters for ionic and each electronic excited state individually if at all such data are available.

F. MC trajectory calculations using the inputs calculated by Olson, Peterson, and Moseley[27]

In addition to the Ne – Cl ion pair, He – H can be used to demonstrate the validity of the current trajectory simulation approach to predict experimental observables using quantum level information as inputs. Most importantly, quantum calculations are self-consistent and when coupled with classical trajectory simulations (Langevin Dynamics or Molecular Dynamics) allow holistic investigation of the effect of ion composition as well as gas pressure and temperature on recombination kinetics. Furthermore, the trajectory simulation approach is amenable to the inclusion of more chemical physics into the modeling such as de-excitation rules, vibrational and rotational transitions, splitting of energy levels due to externally applied electromagnetic fields, to name a few. For instance, an excited state after formation can be allowed to de-excite (through collisional interactions or by photoemission) at rates that are experimentally measured or computed from first principles. Such an extension could potentially improve the accuracy of predictions and would make comparison with experimental data on MN reactions more direct. While adopting the trajectory simulation-based approach advanced here, one must also be aware of the difficulties when trying to do quantum chemical calculations that provide key inputs for the classical trajectory simulations. For the ion pair $He^+ - H^-$, all excited states of He have energy levels below the dissociation limit with estimated crossing distances, shown in Table S2-D. To describe the highest excited state of He alone, a minimum of nine orbitals are required. However, targeting specific states in MOLPRO is challenging. For the He – H system, states with A_1 symmetry (C_{2v} group) are desired for obtaining all the $^1\Sigma^+$ states where the transition between ionic and neutral states occur. However, states associated with the excited H atom must satisfy the wave function symmetry constraint and electron number constraint as well. For example, $He\left(1s^2\right) + H\left(2s^1\right)$ and $He\left(1s^2\right) + H\left(2p^1\right)$ satisfy the constraints perfectly and these two states have lower energy levels than the ion dissociation limit. In fact, excited states of H atom up to its ionization limit are all satisfactory. Beyond the ionization limit of H, due to the constraint on the system electron number, the "reverse" ionized states such as $He^-\left(1s^2\,2s^1\right) + H^+$ and $He^-\left(1s^2\,3s^1\right) + H^+$ are populated as well. Even a small system such as He – H exhibits this complexity more commonly seen in other combinations of rare gas cations R^+ recombining with halide anions X^- such as for instance, $Ne^+ - Cl^-$. Unfortunately, we are not aware

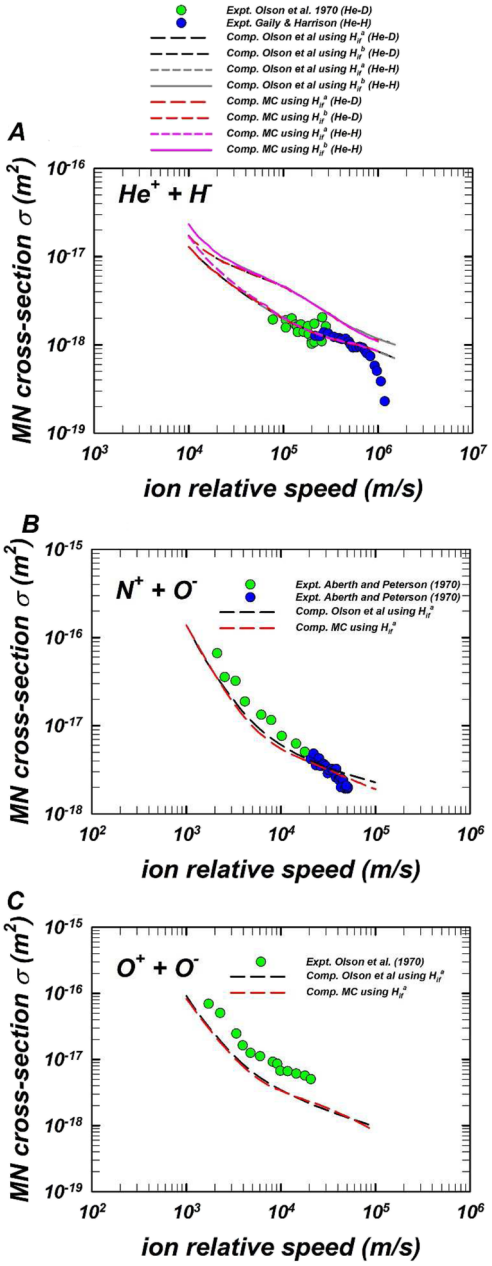

FIG. 12. (a) He – H MN cross section $\sigma(v)$. Experimental data ("Expt.") reported by Olson, Peterson, and Moseley[27] and Gaily and Harrison[25] are plotted. Computations ("Comp.") reported by Olson, Peterson, and Moseley[27] computed using two parameterizations: H_{if}^a and H_{if}^b for He – H and He – D pairs. MC trajectory simulation calculations using the H_{if}^a and H_{if}^b He – H and He – D pairs are reported to show the equivalence of both the approaches. (b) N – O MN cross section $\sigma(v)$. Experimental data ("Expt.") reported by Aberth and Peterson[26] are plotted. Computations ("Comp.") reported by Olson, Peterson, and Moseley[27] computed using H_{if}^a developed by Olson, Smith, and Bauer[48] as well as the MC calculations using H_{if}^a are plotted. (c) O – O MN cross section $\sigma(v)$. Experimental data ("Expt.") reported by Olson, Peterson, and Moseley[27] are plotted. Computations ("Comp.") reported by Olson, Peterson, and Moseley[27] computed using H_{if}^a developed by Olson, Smith, and Bauer[48] as well as the MC calculations using H_{if}^a are plotted.

of a solution to this issue. Intuitive ways to prevent the population of reverse ionized states in electronic structure calculations need to be incorporated in the future work.

To further demonstrate the ability of the current approach to yield accurate cross sections and product branching ratios, we use H_{12} calculations provided by Olson, Peterson, and Moseley[27] and compute $\sigma(v)$ for three ion pairs: $He^+ - H^-, N^+ - O^-$, $O^+ - O^-$. Olson, Peterson, and Moseley[27] computed cross sections and product branching ratios analytically, which we reproduce using trajectory simulations. The intention here is to demonstrate that trajectory simulations are consistent with Olson's analytical approach while being also amenable for building complexity in the chemical systems modeled by incorporating additional physical models as desired.

G. $He^+ - H^-$ ion pair

For the $He^+ - H(D)^-$ ion pair, there are ten product channels or states whose energy is within the ion dissociation limit. A summary of the associated He atomic state of each channel can be found in Table S2-D, wherein two sets of coupling values H_{if}^a and H_{if}^b reported by Olson, Peterson, and Moseley[27] are tabulated and checked against the current simulation method. H_{if}^a set was computed using the regression fit for one electron transfer systems developed by Olson, Smith, and Bauer[48] and H_{if}^b set was calculated using an analytical solution originally derived by Smirnov.[107,108] The comparison with Olson's direct integration is shown in Fig. 12(a) for partial cross section and in Table X for the product branching ratio (only the nonzero channels are shown). The cross section calculation shows perfect agreement with the direct integral and the branching ratio result has a maximum difference of 1.6% for both sets of coupling values H_{if}^a and H_{if}^b.

H. $N^+ - O^-$ ion pair

For the $N^+ - O^-$ ion pair, it is experimentally observed that both excited state of nitrogen and that of oxygen are populated after the neutralization reaction and at thermal energies the excited state of nitrogen is strongly preferred. According to Olson, Peterson, and Moseley,[27] a total of 19 states including ten excited states of nitrogen, eight excited states of oxygen, and one excited state of both nitrogen and oxygen have associated energy levels below the ion dissociation limit and are summarized in Table S2-E. It is then necessary to identify the permissible atomic states for each of six molecular states ($^{2,4}\Sigma$, $^{2,4}\Pi$, and $^{2,4}\Delta$) and calculate cross sections of each molecular state, and the result is obtained as a weighted average of each of six cross sections. For a diatomic system where both atoms have negligible spin–orbit coupling such as N – O, the allowable molecular states are calculated as all combinations of the L and S quantum numbers of the two separated atoms. The final Λ (the projection of orbital angular momentum along the internuclear axis) is computed as $\Lambda = |M_{L1} + M_{L2}|$, where M_{L1} and M_{L2} rise from each individual atom and the total spin quantum number S can take values from $(S_1 + S_2)$ to $|S_1 - S_2|$. The weightage factor for each molecular state that the two ions can form are calculated by computing the frequency or the total number of degenerate states for each combination of Λ and spin multiplicity $2S + 1$ divided by the total frequency. As an example, N^+ and O^- ions have atomic terms of ^3P and ^2P with $M_L = 1, 0, -1$ for both. The possible resultant M_L values for the diatomic system are $-2, -1, 0, 1, 2$, where $|M_L| = 0, 1, 2$ denotes the Σ, Π, Δ states, respectively. For N – O, the frequency of Σ, Π, Δ states is 3, 4, 2, respectively. The total spin quantum number could take values of $\frac{3}{2}$ and $\frac{1}{2}$, which corresponds to spin multiplicities of 4 and 2. Finally, the six permissible molecular states are $^2\Sigma, ^2\Pi, ^2\Delta, ^4\Sigma, ^4\Pi, ^4\Delta$ with weighting factors of $\frac{6}{54}, \frac{8}{54}, \frac{4}{54}, \frac{12}{54}, \frac{16}{54}, \frac{8}{54}$. Following the same principle, for each combination of atomic states listed in Table S2-E, we determine if the molecular states caused by excited atomic states are included in the molecular states caused by the ions ($^2\Sigma, ^2\Pi, ^2\Delta, ^4\Sigma, ^4\Pi, ^4\Delta$). If not, the R_x and H_{if} values for such a combination are excluded in the calculation of that molecular state. A comparison between the direct integral and the simulation method can be found in Fig. 12(b) for cross sections and Table XI for the branching ratio (only nonzero channels are shown). We observe that the Monte Carlo method gives a smaller cross section for higher energy collisions than in the experiment.

I. $O^+ - O^-$ ion pair

Like the $N^+ - O^-$ ion pair, multiple molecular states are involved in the neutralization of $O^+ - O^-$, which are $^{3,5}\Sigma$ and $^{3,5}\Pi$. The permissible atomic state for each molecular state is first identified and followed by a calculation of four cross sections that are later weighted to calculate the total cross section. A summary of atomic state involved is shown in Table S2-F, and a comparison of the current method with Olson's direct integral (following the weighting method described for N – O) can be found in Fig. 12(c) and Table XII for cross section and branching ratio, respectively. Both

TABLE X. He − H branching ratio comparison.

State of He	(%) 300 K using H_{if}^a	MC simulation (%)	(%) 300 K using H_{if}^b	MC simulation (%)
$3s\ ^3S$	41.0	40.8	6.5	6.7
$3s\ ^1S$	26.7	27.5	28.0	28.4
$3p\ ^3P$	14.3	14.1	29.7	29.9
$3d\ ^3D$	6.0	5.9	7.8	7.5
$3d\ ^1D$	6.0	6.1	7.8	9.0
$3p\ ^1P$	6.0	5.5	20.2	18.6

TABLE XI. N − O branching ratio comparison.

State of N	State of O	Olson 300 K (%)	MC simulation (%)
$3p\ ^2S$	$2p^4\ ^3P$	1.5	2.3
$3p\ ^4D$	$2p^4\ ^3P$	17.5	14.7
$3p\ ^4P$	$2p^4\ ^3P$	26.7	22.2
$2p^3\ ^4S$	$4s\ ^5S$	2.7	5.4
$2p^3\ ^4S$	$4s\ ^3S$	2.8	5.6
$3p\ ^4S$	$2p^4\ ^3P$	7.1	10.6
$3p\ ^2D$	$2p^4\ ^3P$	16.6	15.2
$2p^3\ ^4S$	$3d\ ^5D$	9.9	9.1
$2p^3\ ^4S$	$3d\ ^3D$	8.6	8.5
$3p\ ^2P$	$2p^4\ ^3P$	5.8	5.5
$2p^3\ ^4S$	$4p\ ^5P$	0.3	0.4
$3s\ ^4P$	$2p^4\ ^1D$	0.5	0.3
$2p^3\ ^4S$	$4p\ ^3P$	0.0	0.1
$3s'\ ^2D$	$2p^4\ ^3P$	0.0	0.1

TABLE XII. O − O branching ratio comparison.

State of O		Olson 300 K (%)	MC simulation (%)
$3p\ ^5P$	$2p^4\ ^3P$	33.6	32.0
$3p\ ^3P$	$2p^4\ ^3P$	58.0	54.2
$3s\ ^5S$	$2p^4\ ^1D$	8.4	13.7

cross section result and branching ratio results of the MC simulation show excellent agreement with the direct integral.

IV. CONCLUSIONS

In this computational study, we have extended Olson's absorbing sphere model,[44] which invokes the Landau–Zener transition state theory[45–47] to estimate the probability of electron transfer between two ions, to include the effect of neutral gas pressure on MN reactions. We incorporated the probability of electron transfer into classical trajectory simulations (Monte Carlo simulations in vacuum and Langevin Dynamics simulations at finite pressures) and showed that our approach is equivalent to the absorbing sphere model. We carried out detailed electronic structure calculations using MOLPRO to obtain PECs from which two inputs to the Landau–Zener theory, namely, R_x and H_{if}, are derived for the subsequent self-consistent calculation of p_{LZ} for the considered ion pair. The key advantage of our trajectory simulation approach is that it is amenable to the inclusion of chemical physics beyond what was considered by Olson,[27,44] for instance, like our inclusion of the effect of ion-neutral interactions on MN. For small monoatomic ion pairs such as $H^+ - H^-$ and $Li^+ - H(D)^-$, we showed that our approach excellently reproduces MN reaction cross section calculations of Olson, Peterson, and Moseley[27] and quantitatively agrees with corresponding experimental data.[21–24,91] For the larger monoatomic ion pair $Ne^+ - Cl^-$, our predictions of the MN rate constant at ~1 Torr are a factor of ~2 to 3 higher than experimentally measured value.[15] Similarly, for $Xe^+ - F^-$ in the pressure range of $\sim(2-8)\times10^4$ Pa, our predictions of the MN rate constant are ~20% lower and are in qualitative agreement with experimental data.[61] In both instances of these larger monoatomic ion pairs, the accuracy of our electronic structure calculations are only moderate and need to be further improved by better treatment of spin–orbit couplings in these chemical systems.

We attribute the differences seen in relatively complex chemical systems such as $Ne^+ - Cl^-$, $Xe^+ - F^-$ to the non-inclusion of system-specific chemical physics such as de-excitation also in addition to the accuracy of implementation of the Landau–Zener theory itself in which we acknowledge that there are several outstanding quantum computational challenges that need to be resolved in the future work. Olson, Peterson, and Moseley[27] originally applied Landau–Zener theory for chemical systems involving one electron transfer. Olson's correlation[48] for $H_{if}(R_x)$ has been widely used,[52] even though it was developed based on small species with a fewer number of electrons. We have pursued electronic structure calculations in this study instead of using Olson's correlation. Our approach can be further improved in subsequent studies, especially probing the monoatomic ion pairs with greater rigor in quantum calculations. We conclude that the current study sets up a computing paradigm for modeling MN reactions to self-consistently capture the effect of gas pressure while offering scope for the inclusion of additional chemical physics such as de-excitation kinetics, the effect of external electric and magnetic fields, and chemical systems with multiple state interactions as opposed to the two state interaction treatment applied here. While considering additional factors that may affect the quantum mechanics of electron transfer, a more sophisticated methodology of capturing the probability of electron transfer may be necessary, but we consider that the core approach of incorporating the same into classical trajectory simulations remains valid.

SUPPLEMENTARY MATERIAL

Section S1. Lennard-Jones (LJ) parameters for atomic species and ion friction factors. Section S2. Additional information related to electronic structure calculations.

ACKNOWLEDGMENTS

Funding for this research was provided by the US Department of Energy Award No. DE-SC0021246 from the Office of Basic Energy Sciences for all authors. Additional support for NJD was provided by NSF Grant No. CHE-2154121. The University of Memphis High Performance Computing Center provided computational resources. The authors thank Professor Carlos Larriba, IUPUI for his guidance in using IMoS software for ion mobility calculations.

AUTHOR DECLARATIONS

Conflict of Interest

The authors have no conflicts to disclose.

Author Contributions

Zhibo Liu: Conceptualization (supporting); Data curation (lead); Formal analysis (lead); Investigation (equal); Methodology (lead);

Software (lead); Validation (lead); Visualization (lead); Writing – original draft (lead). **Mrittika Roy**: Investigation (supporting); Software (supporting). **Nathan J. DeYonker**: Investigation (equal); Methodology (equal); Software (lead); Supervision (supporting). **Ranganathan Gopalakrishnan**: Conceptualization (lead); Data curation (equal); Formal analysis (equal); Funding acquisition (lead); Investigation (equal); Methodology (lead); Project administration (lead); Resources (lead); Supervision (lead); Validation (supporting); Writing – original draft (equal); Writing – review & editing (lead).

DATA AVAILABILITY

The data that support the findings of this study are available from the corresponding author upon reasonable request.

REFERENCES

[1]H. S. W. Massey, Discuss. Faraday Soc. **12**, 24 (1952).
[2]M. Flannery, in *Springer Handbook of Atomic, Molecular, and Optical Physics*, edited by G. Drake (Springer, New York, 2006), p. 799.
[3]L. M. Babcock and N. G. Adams, *Advances in Gas Phase Ion Chemistry* (Elsevier Science, Amsterdam, 2001).
[4]D. R. Bates, in *Advances in Atomic and Molecular Physics*, edited by D. R. Bates and B. Bederson (Academic Press, 1979), p. 235.
[5]M. R. Flannery, in *Advances in Atomic, Molecular, and Optical Physics*, edited by B. Bederson and A. Dalgarno (Elsevier B.V., 1994), Vol. 32, p. 117.
[6]D. Smith, N. G. Adams, and E. Alge, Planet. Space Sci. **29**, 449 (1981).
[7]A. Franchin, S. Ehrhart, J. Leppa, T. Nieminen, S. Gagne, S. Schobesberger, D. Wimmer, J. Duplissy, F. Riccobono, E. M. Dunne, L. Rondo *et al.*, Atmos. Chem. Phys. **15**, 7203 (2015).
[8]J. Kontkanen, K. E. J. Lehtinen, T. Nieminen, H. E. Manninen, K. Lehtipalo, V. M. Kerminen, and M. Kulmala, Atmos. Chem. Phys. **13**, 11391 (2013).
[9]R. P. Turco, F. Q. Yu, and J. X. Zhao, J. Air Waste Manage. Assoc. **50**, 902 (2000).
[10]R. P. Turco, J. X. Zhao, and F. Q. Yu, Geophys. Res. Lett. **25**, 635, https://doi.org/10.1029/98gl00253 (1998).
[11]N. G. Adams and D. Smith, Contemp. Phys. **29**, 559 (1988).
[12]D. R. Bates, J. Phys. B: At. Mol. Phys. **13**, 205 (1980).
[13]D. R. Bates, Planet. Space Sci. **30**, 1275 (1982).
[14]D. Smith and N. G. Adams, Geophys. Res. Lett. **9**, 1085, https://doi.org/10.1029/gl009i009p01085 (1982).
[15]N. S. Shuman, T. M. Miller, R. Johnsen, and A. A. Viggiano, J. Chem. Phys. **140**, 044304 (2014).
[16]I. M. Littlewood, J. Phys. D: Appl. Phys. **23**, 308 (1990).
[17]V. I. Molotkov, H. M. Thomas, A. M. Lipaev, V. N. Naumkin, A. V. Ivlev, and S. A. Khrapak, Int. J. Microgravity Sci. Appl. **32**, 320302 (2015).
[18]D. A. Armstrong, Radiat. Phys. Chem. **20**, 75 (1982).
[19]D. E. Wilson, W. J. Quiring, and D. A. Armstrong, J. Appl. Phys. **47**, 1194 (1976).
[20]M. Stenrup, Å. Larson, and N. Elander, Phys. Rev. A **79**, 012713 (2009).
[21]B. Peart and D. A. Hayton, J. Phys. B: At., Mol. Opt. Phys. **27**, 2551 (1994).
[22]S. Szucs, M. Karemera, M. Terao, and F. Brouillard, J. Phys. B: At. Mol. Phys. **17**, 1613 (1984).
[23]J. Moseley, W. Aberth, and J. R. Peterson, Phys. Rev. Lett. **24**, 435 (1970).
[24]R. D. Rundel, K. L. Aitken, and M. F. A. Harrison, J. Phys. B: At. Mol. Phys. **2**, 954 (1969).
[25]T. D. Gaily and M. F. A. Harrison, J. Phys. B: At. Mol. Phys. **3**, 1098 (1970).
[26]W. H. Aberth and J. R. Peterson, Phys. Rev. A **1**, 158 (1970).
[27]R. E. Olson, J. R. Peterson, and J. Moseley, J. Chem. Phys. **53**, 3391 (1970).
[28]J. P. Wiens, N. S. Shuman, T. M. Miller, and A. A. Viggiano, J. Chem. Phys. **144**, 204309 (2016).
[29]N. S. Shuman, A. A. Viggiano, and R. Johnsen, J. Chem. Phys. **138**, 204302 (2013).
[30]N. S. Shuman, T. M. Miller, A. A. Viggiano, and J. Troe, in *Advances in Atomic, Molecular, and Optical Physics*, edited by P. Berman, E. Arimondo, and C. Lin (Academic Press, 2012), p. 209.
[31]N. S. Shuman, T. M. Miller, R. Bemish, and A. A. Viggiano, J. Phys.: Conf. Ser. **300**, 012007 (2011).
[32]T. M. Miller, J. F. Friedman, and A. A. Viggiano, Int. J. Mass Spectrom. **267**, 190 (2007).
[33]N. S. Shuman, J. P. Wiens, T. M. Miller, and A. A. Viggiano, J. Chem. Phys. **140**, 224309 (2014).
[34]J. P. Wiens, N. S. Shuman, and A. A. Viggiano, J. Chem. Phys. **142**, 114304 (2015).
[35]J. C. Sawyer, T. M. Miller, B. C. Sweeny, S. G. Ard, A. A. Viggiano, and N. S. Shuman, J. Chem. Phys. **149**, 044303 (2018).
[36]N. S. Shuman, T. M. Miller, C. M. Caples, and A. A. Viggiano, J. Phys. Chem. A **114**, 11100 (2010).
[37]N. S. Shuman, T. M. Miller, N. Hazari, E. D. Luzik, and A. A. Viggiano, J. Chem. Phys. **133**, 234304 (2010).
[38]T. M. Miller, J. F. Friedman, N. S. Shuman, S. G. Ard, J. J. Melko, and A. A. Viggiano, J. Phys. Chem. A **116**, 10293 (2012).
[39]D. Smith, N. G. Adams, and M. J. Church, Planet. Space Sci. **24**, 697 (1976).
[40]D. Smith and M. J. Church, Int. J. Mass Spectrom. Ion Phys. **19**, 185 (1976).
[41]D. Smith, N. G. Adams, and M. J. Church, J. Phys. B: At. Mol. Phys. **11**, 4041 (1978).
[42]D. Smith and M. J. Church, Planet. Space Sci. **25**, 433 (1977).
[43]M. Tsuji, H. Ishimi, and Y. Nishimura, Chem. Lett. **25**, 515 (1996).
[44]N. J. Kruse and G. J. Small, J. Chem. Phys. **56**, 2985 (1972).
[45]C. Wittig, J. Phys. Chem. B **109**, 8428 (2005).
[46]C. Zener and R. H. Fowler, Proc. R. Soc. London, Ser. A **137**, 696 (1932).
[47]D. R. Bates, Proc. R. Soc. London, Ser. A **257**, 22 (1960).
[48]R. E. Olson, F. T. Smith, and E. Bauer, Appl. Opt. **10**, 1848 (1971).
[49]R. E. Olson and A. Salop, Phys. Rev. A **14**, 579 (1976).
[50]H. B. Gilbody, J. B. Hasted, and H. S. W. Massey, Proc. R. Soc. London, Ser. A **238**, 334 (1997).
[51]A. P. Hickman, J. Chem. Phys. **70**, 4872 (1979).
[52]J. C. Bopp, T. M. Miller, A. A. Viggiano, and J. Troe, J. Chem. Phys. **129**, 074308 (2008).
[53]R. E. Olson, Int. J. Quantum Chem. **24**, 49 (2009).
[54]*Pure and Applied Physics*, edited by S. Geltman (Elsevier, 1969), p. 213.
[55]*Pure and Applied Physics*, edited by S. Geltman (Elsevier, 1969), p. 222.
[56]J. C. Keck, J. Chem. Phys. **32**, 1035 (2004).
[57]E. Wigner, J. Chem. Phys. **5**, 720 (2004).
[58]G. Y. Zhu, Y. Qin, M. Meng, S. Mallick, H. Gao, X. Chen, T. Cheng, Y. N. Tan, X. Xiao, M. J. Han, M. F. Sun, and C. Y. Liu, Nat. Commun. **12**, 456 (2021).
[59]S. Chandrasekhar, Rev. Mod. Phys. **15**, 1 (1943).
[60]N. J. Kasdin, J. Gui., Control, Dyn. **18**, 114 (1995).
[61]H. S. Lee and R. Johnsen, J. Chem. Phys. **93**, 4868 (1990).
[62]H. S. Lee and R. Johnsen, J. Chem. Phys. **90**, 6328 (1989).
[63]H. Jungblut, D. Hansen, and W. F. Schmidt, IEEE Trans. Electr. Insul. **24**, 343 (1989).
[64]H. P. Gunawardena, M. He, P. A. Chrisman, S. J. Pitteri, J. M. Hogan, B. D. M. Hodges, and S. A. McLuckey, J. Am. Chem. Soc. **127**, 12627 (2005).
[65]J. M. Wells, P. A. Chrisman, and S. A. McLuckey, J. Am. Chem. Soc. **125**, 7238 (2003).
[66]V. Suresh and R. Gopalakrishnan, J. Aerosol Sci. **155**, 105746 (2021).
[67]R. Kubo, Rep. Prog. Phys. **29**, 255 (1966).
[68]C. Larriba and C. J. Hogan, J. Phys. Chem. A **117**, 3887 (2013).
[69]C. Larriba and C. J. Hogan, J. Comput. Phys. **251**, 344 (2013).
[70]C. Larriba-Andaluz and C. J. Hogan, Jr., J. Chem. Phys. **141**, 194107 (2014).
[71]C. Larriba-Andaluz, J. Fernández-García, M. A. Ewing, C. J. Hogan, and D. E. Clemmer, Phys. Chem. Chem. Phys. **17**, 15019 (2015).

[72]V. Shrivastav, M. Nahin, C. J. Hogan, and C. Larriba-Andaluz, J. Am. Soc. Mass Spectrom. **28**, 1540 (2017).
[73]L. Li and R. Gopalakrishnan, J. Aerosol Sci. **151**, 105678 (2021).
[74]L. Li, H. S. Chahl, and R. Gopalakrishnan, J. Aerosol Sci. **140**, 105481 (2020).
[75]H. S. Chahl and R. Gopalakrishnan, Aerosol Sci. Technol. **53**, 933 (2019).
[76]R. Gopalakrishnan, P. H. McMurry, and C. J. Hogan, Aerosol Sci. Technol. **49**, 1181 (2015).
[77]R. Gopalakrishnan, T. Thajudeen, H. Ouyang, and C. J. Hogan, J. Aerosol Sci. **64**, 60 (2013).
[78]R. Gopalakrishnan, M. J. Meredith, C. Larriba-Andaluz, and C. J. Hogan, J. Aerosol Sci. **63**, 126 (2013).
[79]V. Suresh, L. Li, J. Redmond Go Felipe, and R. Gopalakrishnan, J. Phys. D: Appl. Phys. **54**, 275205 (2021).
[80]V. Madugula, V. Suresh, Z. Liu, D. R. Ballard, L. D. Wymore, and R. Gopalakrishnan, "Self-consistent calculations of the electric charge, ion drag force, and the drift velocity of spherical grains using Langevin Dynamics and comparisons against canonical experiments" (unpublished).
[81]P. J. Knowles and N. C. Handy, Chem. Phys. Lett. **111**, 315 (1984).
[82]P. J. Knowles and N. C. Handy, Comput. Phys. Commun. **54**, 75 (1989).
[83]T. H. Dunning, Jr., J. Chem. Phys. **90**, 1007 (1989).
[84]B. P. Prascher, D. E. Woon, K. A. Peterson, T. H. Dunning, and A. K. Wilson, Theor. Chem. Acc. **128**, 69 (2011).
[85]K. A. Peterson, D. Figgen, E. Goll, H. Stoll, and M. Dolg, J. Chem. Phys. **119**, 11113 (2003).
[86]See, https://www.molpro.net/manual/doku.php?id=basis_input & s[]=even for basis input.
[87]J. Emsley, *The Elements* (Clarendon Press, 1998).
[88]See https://physics.nist.gov/PhysRefData/Handbook/Tables/hydrogentable1.htm for Basic Atomic Spectroscopic Data for Hydrogen (H).
[89]L. J. Radziemski, R. Engleman, and J. W. Brault, Phys. Rev. A **52**, 4462 (1995).
[90]G. Herzberg and H. R. Moore, Can. J. Phys. **37**, 1293 (1959).
[91]T. Launoy, J. Loreau, A. Dochain, J. Liévin, N. Vaeck, and X. Urbain, Astrophys. J. **883**, 85 (2019).
[92]Y. Gim and C.-W. Lee, J. Chem. Phys. **141**, 144313 (2014).
[93]S. R. Langhoff and E. R. Davidson, Int. J. Quantum Chem. **8**, 61 (1974).
[94]L. Meissner, Chem. Phys. Lett. **146**, 204 (1988).
[95]See https://physics.nist.gov/PhysRefData/Handbook/Tables/neontable1.htm for Basic Atomic Spectroscopic Data for Neon (Ne).
[96]See https://physics.nist.gov/PhysRefData/Handbook/Tables/chlorinetable1.htm for Basic Atomic Spectroscopic Data for Chlorine (Cl).
[97]L. J. Radziemski and V. Kaufman, J. Opt. Soc. Am. **59**, 424 (1969).
[98]G. E. Uhlenbeck and L. S. Ornstein, Phys. Rev. **36**, 823 (1930).
[99]W. R. Harper, Math. Proc. Cambridge Philos. Soc. **28**, 219 (1932).
[100]F. Brandi, I. Velchev, W. Hogervorst, and W. Ubachs, Phys. Rev. A **64**, 032505 (2001).
[101]J. E. Hansen and W. Persson, Phys. Scr. **36**, 602 (1987).
[102]G. A. Laguna and W. H. Beattie, Chem. Phys. Lett. **88**, 439 (1982).
[103]See https://physics.nist.gov/PhysRefData/Handbook/Tables/fluorinetable1.htm for Basic Atomic Spectroscopic Data for Fluorine (F).
[104]See https://physics.nist.gov/PhysRefData/Handbook/Tables/xenontable1.htm for Basic Atomic Spectroscopic Data for Xenon (Xe).
[105]B. Zhang, J. E. Vandezande, R. D. Reynolds, and H. F. Schaefer III, J. Chem. Theory Comput. **14**, 1235 (2018).
[106]See https://www.molpro.net/manual/doku.php?id=spin-orbit-coupling & s[]=spin & s[]=orbit for Spin-orbit-coupling [Molpro manual].
[107]B. M. Smirnov, Dokl. Akad. Nauk SSSR **173**, 316 (1967) [Sov. Phys. Dokl. **12**, 242 (1967)].
[108]B. M. Smirnov, Dokl. Akad. Nauk SSSR **161**, 92 (1965) [Sov. Phys. Dokl. **10**, 218 (1965)].
[109]See https://physics.nist.gov/PhysRefData/Handbook/Tables/lithiumtable1.htm for Basic Atomic Spectroscopic Data for Lithium (Li).
[110]H. Croft, A. S. Dickinson, and F. X. Gadéa, Mon. Not. R. Astron. Soc. **304**, 327 (1999).